ACS OMEGA

Open Access

http://pubs.acs.org/journal/acsodf

Article

Discovery of Potential Inhibitors of CDK1 by Integrating Pharmacophore-Based Virtual Screening, Molecular Docking, Molecular Dynamics Simulation Studies, and Evaluation of Their Inhibitory Activity

Vineeta Teotia, Prakash Jha, and Madhu Chopra*

Cite This: *ACS Omega* 2024, 9, 39873−39892

Read Online

ACCESS | Metrics & More | Article Recommendations | Supporting Information

ABSTRACT: The ability of CDK1 to compensate for the absence of other cell cycle CDKs poses a great challenge to treat cancers that overexpress these proteins. Despite several studies focusing on the area, there are no FDA-approved drugs selectively targeting CDK1. Here, the study aimed to develop potential CDK1 selective inhibitors through drug repurposing and leveraging the structural insights provided by the hit molecules generated. Approximately 280,000 compounds from DrugBank, Selleckchem, Otava and an in-house library were screened initially based on fit values using 3D QSAR pharmacophores built for CDK1 and subsequently through Lipinski, ADMET, and TOPKAT filters. 10,310 hits were investigated for docking into the binding site of CDK1 determined using the crystal structure of human CDK1 in complex with NU6102. The best 55 hits with better docking scores were further analyzed, and 12 hits were selected for 100 ns MD simulations followed by binding energy calculations using the MM-PBSA method. Finally, 10 hit molecules were tested in an *in vitro* CDK1 Kinase inhibition assay. Out of these, 3 hits showed significant CDK1 inhibitory potential with IC_{50} < 5 μM. These results indicate these compounds can be used to develop subtype-selective CDK1 inhibitors with better efficacy and reduced toxicities in the future.

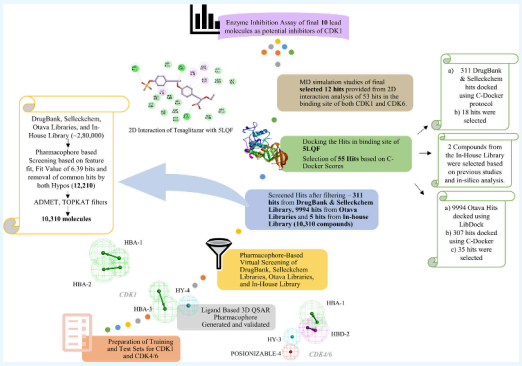

1. INTRODUCTION

Deregulation of the cell cycle and its proteins leads to the transformation of normal cells to tumorigenic cells. Cell cycle proteins consist mainly of cyclin-dependent kinases (CDKs) and their activating partners called cyclins.[1] CDKs are serine/threonine protein kinases that form a complex with corresponding cyclins to phosphorylate various substrates for smooth cell cycle progression. Apart from this, CDKs also play a role in transcription, epigenetics, angiogenesis, hematopoiesis, metabolism, neuronal activity, spermatogenesis and DNA repair.[2] Increased expression of CDKs and cyclins along with decreased expression of endogenous CDK inhibitors like CIP/KIP or INK4 are observed in multiple types of malignancies. Therefore, CDKs are considered to be an important target for anticancer therapy.[3]

Human CDKs are mainly divided into two subclasses, the cell cycle CDKs (CDK1, 2, 4, and 6) and the transcriptional CDKs (CDK7, 8, 9, 12, and 13). However, some other CDKs like CDK5, 10, 11, 14−18, and 20 have diverse, unique and tissue-specific functions.[4−6] Among the main interphasic CDKs, CDK1 has been established as most essential to carry out the smooth progression of a cell cycle as it can bind to not only cyclins A and B but also cyclins D and E to some extent in the absence of CDK4/6 and CDK2, respectively.[7,8] CDK1 comprises 297 amino acid residues characterized by a single catalytic serine/threonine kinase domain.[9,10] It has a two-lobed structure consisting of an active site between an N-terminal lobe made up of β-sheets and a C-terminal lobe made up of α-helices. The N-terminal lobe possesses a glycine-rich inhibitory element called the G-Loop and the C-helix, also known as the PSTAIRE helix. The C-terminal lobe has an activation segment ranging from the DFG motif to the APE motif plus the T-loop that covers the catalytic cleft in an unbound CDK1.[11]

In addition to cell cycle regulation, CDK1 also has a role in transcription by phosphorylating RNAPII,[12] takes part in epigenetic regulation through interaction with EZH2, is a part of HR-mediated DNA damage repair, causes myoblast proliferation,[13] regulates cell adhesion,[14] represses autophagy in mitosis,[15] and takes part in cell metabolism.[16,17]

The expression level of CDK1 is found to be altered in all major types of cancers[18−27] and in neurodegenerative disorders

Received: June 10, 2024
Revised: August 26, 2024
Accepted: August 29, 2024
Published: September 13, 2024

like Parkinson's disease[28] and Alzheimer's.[29] Targeting CDK1 is also considered a potential strategy to treat tumors overexpressing MYC, a proto-oncogene due to its undruggable nature.[30] Due to these reasons, developing specific inhibitors for CDK1 could play an important role in designing new strategies for the treatment of cancer and other diseases.[31]

To date, many pan-CDK inhibitors have been developed out of which some have been FDA approved while others are in clinical trials.[4] One of the first-generation pan-CDK inhibitors, Flavopiridol, is an FDA-approved orphan drug for chronic lymphocytic leukemia;[32] other CDK inhibitors targeting multiple CDKs under trial include Roscovitine, Dinaciclib, P276−00, Roniciclib, AT7519, R547, SNS-032, and Milciclib.[33] Due to the limited efficacy, increased toxicity associated with nonselective CDK inhibitors, lack of clear understanding of the mechanism of action and nonachievement of the therapeutic window of these drugs for discrimination between cancerous and normal tissues, designing of selective CDK inhibitors is the key to their successful usage as therapeutic agents.[34] To this effect, three CDK4/6 selective inhibitors, Palbociclib, Ribociclib, and Abemaciclib,[35] have been approved by the U.S. FDA for use in breast cancer therapies.[33] Recently, a fourth CDK4/6 selective inhibitor Trilaciclib has been approved by U.S. FDA for small-cell lung carcinoma.[35] In a study utilizing CDK1 conditional knockout mice, it was observed that tumors did not propagate in the absence of CDK1 and CDK1 inhibitors can be beneficial for cancer therapy provided the interference in essential functions of this protein in proliferating tissues can be prevented.[36] Also, it is suggested in a report that cancer cells may be more sensitive to CDK1 inhibition, where downregulation of its expression will trigger CDK2-mediated mitosis, leading to the death of the majority of the cells during the defective mitotic cycle or at the next interphase stage. However, in normal tissues, cells could be arrested at the G_2 stage, and they might re-enter the cell cycle after restoration of CDK1 expression.[37] To date, there has not been much success in the development of CDK1 subtype-specific inhibitors, for example, RO-3306, a CDK1 inhibitor that has failed due to rapid clearance from the blood plasma.[38] Therefore, the development of drugs that selectively target CDK1 is much needed.

Drug repurposing based on computational approaches like signature matching, molecular docking, genetic association, pathway mapping, retrospective clinical analysis, and novel data sources has become a major strategy to identify new targets for approved or investigational drugs apart from their original use.[39] This strategy helps accelerate the drug discovery process, as the pharmacokinetic properties and toxicity profile of these drugs are known; it also helps reduce the costs involved in research for a new compound. To date, various computational drug design strategies have been employed in the development of CDK1 inhibitors. A few of them include screening of libraries like NCI, Maybridge, and in-house libraries using a pharmacophore model developed using a single series of compounds and evaluating their CDK1 activity *in vitro*,[40] docking the screened compounds in the binding site of homology-modeled CDK1 structure when X-ray crystal structure was unavailable,[41] docking studies of flavonoids, natural compounds, phytochemicals, and dinaciclib analogs as CDK1 inhibitors,[42−46] and screening of in-house libraries using denovo drug design approaches.[47]

In the present study, a diverse set of molecules from 16 different series of compounds were used to build a ligand-based 3D QSAR pharmacophore model for CDK1. Multiple computational drug screening strategies were employed in a systematic manner to identify potent CDK1 inhibitors. High-throughput virtual screening (HTVS) of DrugBank (DB),[48] Selleckchem (SC),[49] Otava libraries,[50] and one in-house synthetic library[51] with the help of a generated pharmacophore model followed by molecular docking was performed to generate hits with better scores against CDK1. These hits were then subjected to molecular dynamics (MD) simulation studies to assess their stability as complexes, followed by estimating binding affinities using MM-PBSA. The final eight hit molecules were further tested in an enzyme inhibition assay to evaluate their *in vitro* CDK1 inhibitory activity. We also tested top hit compounds from an in-house series of 1,3,4-oxadiazole thiones for their CDK1 inhibitory activity developed previously as anticancer agents in our lab.[51] The observations drawn from this study can be utilized in future research to explore their potential as CDK1 selective inhibitors to be used in clinics in cancer therapy.

2. MATERIAL AND METHODS

2.1. Software. Biovia Discovery Studio 2021 was used to build pharmacophore models and to perform virtual screening and docking studies. MD simulation studies were carried out in GROMACS 2019.2.[52,53] The structures of the compounds were drawn using MarvinSketch 19.20 of ChemAxon Ltd.[54]

2.2. Preparation of Data Sets. Building a robust pharmacophore model begins with selecting a structurally diverse set of compounds for the data set curation. The range of activity data of these compounds should span 4−5 orders of magnitude. The data set should be devoid of structural or activity data redundancy, making this the crucial initial step in model development.[55] Here, a set of more than 62 inhibitors of CDK1 of 16 different series of compounds with their biological data was obtained from the literature.[56−71] This set was manually divided into a training set and test set of 35 and 27 compounds, respectively, after careful examination of structural diversity and non-redundancy (The chemical structures of the training set and test set compounds are enumerated in Chart S1 and Chart S2). Based on the activity scale, compounds with IC_{50} values less than 60 nM were categorized as actives, 60−1000 nM were categorized as moderately active, and greater than 1000 nM were categorized as inactive compounds for CDK1. A wide range of activity ensures that all critical information is used by the algorithm to generate the best feature pharmacophore. The uncertainty value (ratio of the range of the activity values of the compounds) was set to 3 (default). To establish the selective nature of CDK1 pharmacophore, a comparable CDK4/6 pharmacophore was also generated using a set of 105 CDK4/6 inhibitors from 12 structurally diverse series of compounds with their wide range of biological activity data from the literature.[72−83] In the case of CDK4/6, the training set and test set consisted of 59 and 46 compounds, respectively (Chart S3 and Chart S4). Compounds with IC_{50} values less than or equal to 20 nM were taken as actives; greater than 20 nM but less than 1000 nM were taken as moderately active; and greater than 1000 nM were taken as inactive compounds for CDK4/6. A pharmacophore model of CDK4/6 was constructed to serve as a validation benchmark for assessing the accuracy of the CDK1 pharmacophore.

2.3. Generation of Pharmacophores. In the present study, the HypoGen algorithm of the Catalyst program, a part

https://doi.org/10.1021/acsomega.4c05414
ACS Omega 2024, 9, 39873−39892

of Biovia's Discovery Studio 2021 v21.1.0.2.298, was used to generate CDK1 and CDK4/6 pharmacophores. All procedures involved in pharmacophore development and validation have been detailed in the previous literature.[55,84,85] In brief, the best quality conformational search tool was used to generate a maximum of 255 conformations of the training set molecules at an energy constraint of 20 kcal mol^{-1} above the global minimum to guarantee that the conformational space is covered maximally. To develop a pharmacophore with the most critical features required, feature mapping was performed on the actives in the data set. Hydrogen bond acceptor (HBA), hydrogen bond donor (HBD), hydrophobic (HY), and ring aromatic (RA) features were selected to build CDK1 pharmacophore. Optimization of the hypothesis was achieved by excluding the ring aromatic feature and removing outlier compounds from the training set with considerable deviation in their estimated activity from the experimental activity. For CDK4/6 pharmacophore, HBA, HBD, HY, and positive ionizable (PosIon) features were used. The maximum number of a particular feature in both the pharmacophores was restricted to 3. The minimum number of features required for a valid pharmacophore was set to 4. These settings and features were used to generate 10 hypotheses each for CDK1 and CDK4/6.

2.4. Validation of Generated Pharmacophores. The top-ranked hypotheses for both CDK1 and CDK4/6 were further validated to check their predictive ability and whether they will be the correct model to screen various databases for active molecules as CDK1 inhibitors.

2.4.1. Cost Function Analysis. HypoGen works on the principle of minimizing the costs of generating the pharmacophore. These costs are calculated in bits. This algorithm calculates a fixed cost (lowest) representing a simple model that fits all data completely and a null cost (highest) representing a model with no features and the highest error. The total cost of a pharmacophore is the sum of three costs, a weight, an error, and a configuration cost. The weight cost measures the deviation of the feature weights from an ideal value of 2. The error cost is dependent on the difference between the estimated activity and the experimental activity. A better correlation coefficient gives a lower RMSD. The configuration cost, also known as the entropy cost gives an idea about the complexity of the hypothesis.[86] A pharmacophore with a configuration cost of less than 17 is considered a good prediction model. The total cost of the pharmacophore should be close to the fixed cost and far from the null cost. For a good hypothesis, a cost difference of 70 and above is considered to provide more than 90% probability of correct prediction.[85] A difference of 40−70 bits between the total cost and the null cost indicates that the model is not generated by chance and has a 70−90% probability of correlation.[87]

2.4.2. Fischer Randomization Method. The CatScramble Test of the Catalyst program in DS was used to perform the Fischer randomization test, which statistically validates the pharmacophore models. In this method, a strong correlation of the activity data with the chemical structures is tested by randomizing the activity of the training set compounds and creating hypotheses with these random training sets.[88] For a statistical significance of 95%, 19 such hypotheses were created with the same features and parameters as those used for the original hypotheses. The original hypothesis is considered effective if it has better cost values, RMS and correlation compared to pharmacophore generated using randomized data sets.

2.4.3. Internal and External Validation Using Training and Test Sets. In addition to predicting activities of the training set, another set of compounds with known activity data is used as a test set to assess the prediction ability of the chosen pharmacophore to categorize them into actives and inactives.[89] A test set of 27 compounds for CDK1 and 46 compounds for CDK4/6 was validated using the Ligand pharmacophore mapping tool in Biovia DS 2021 using the flexible search option of the Best fit method.

2.5. Virtual Screening and Filtration of Initial Hits. Pharmacophore-based virtual screening was performed where the best pharmacophore model was utilized as the 3D search query against a total of 288,671 compounds of DrugBank, Selleckchem databases (Kinase Inhibitors, Natural Products) and Otava libraries (Kinase targeted, Lead-like and Drug-like green collection compounds) using the Screen Library module[88] of DS 2021. The hits from the pharmacophore screening were selected based on a fit value, which was set to 6.39 for CDK1 and 8.9 for CDK4/6. The pharmacophore mapping was used to screen another small synthetic library (15 in number) of 1,3,4-oxadiazole thiones (Table S5) developed previously in our lab as anticancer agents.[51] They were tested for their anticancer activity in four cancer cell lines viz. HeLa, U87, Panc, and MCF-7. Compounds **3i** and **3j** showed the best apoptotic potential in HeLa cervical cancer cell lines, were shown to inhibit cell cycle progression in the G_2-M phase, upregulate the expression of p21 and downregulate the expression of Cyclin B1 therefore, might be active against CDK1. The hits common to both pharmacophore screenings were removed from the hit list to ensure selectivity. Finally, only the compounds that screened out for CDK1 but not for CDK4/6 with the fit value ≥6.39 (CDK1 cutoff); possessing 4 features were selected for future protocols.

As a secondary filter, Lipinski's rule of five and Veber's rule were applied to filter out the drug-like compounds. A compound to pass through these filters should have a molecular weight <500 Da, should not have more than five hydrogen bond donors and ten hydrogen bond acceptors, a log *P* value of ≤5, rotatable bonds of ≤10 and a polar surface area of ≤140 Å.[2,90] The pharmacokinetic properties of the compounds following these rules were examined by submitting them to the ADMET profiler of DS 2021. These properties include absorption, distribution, metabolism, excretion, and blood−brain barrier penetration capabilities. To confirm the safety profile of these compounds, their toxicity analysis was performed using the TOPKAT tool of DS 2021.[91] Hits filtered out from these screens were utilized for further analysis.

2.6. Receptor and Ligand Preparation. To evaluate the binding modes of the screened hits in the active site of CDK1 and revalidate our findings by docking the selected hits in the binding site of CDK6 for selectivity, the protein structures of CDK1 in complex with NU6102 (PDB ID: 5LQF)[92] and CDK6 in complex with Ribociclib (PDB ID: 5L2T)[93] were downloaded from the RCSB protein data bank.[94,95] The proteins were cleaned and prepared by removal of water molecules, addition of hydrogens, adding the missing amino acid residues and loops and correcting bond orders.[96] The screened ligand molecules along with the co-crystallized ligands were prepared using the Prepare Ligand tool in DS 2021. In Ligand Preparation, the ionization states of the ligands were determined, which predicts the predominant

https://doi.org/10.1021/acsomega.4c05414
ACS Omega 2024, 9, 39873−39892

protonation states at physiological pH (6.5−8.5) based on empirical pK_a calculations; the repetitive structures were removed, and the bad valencies of the ligands were fixed by adjusting the charge. Prepared ligands were energy minimized to remove steric clashes, first by steepest descent with an RMS gradient of 0.01 kcal/mol and then by conjugate gradient with an RMS gradient of 0.001 kcal/mol using the CHARMm forcefield.

2.7. Molecular Docking Studies. After the preparation of the protein structure, the docking protocol was validated by redocking the co-crystallized ligands in the respective protein binding sites. The binding grids for both receptors were defined based on co-crystallized ligand site information using the "Define and Edit Binding Site" module in DS 2021. Only one chain "A" was retained besides the co-crystallized ligands. NU6102 and Ribociclib as positive controls were docked using the CDOCKER protocol in DS 2021, in the binding site of CDK1 and CDK6, respectively. The RMSD values of the co-crystallized ligands were calculated after the docking protocol which should be less than 2 Å for successful validation.[97]

Large libraries like Otava were fed to the LibDock module of Discovery Studio for refining the screened molecules.[98] The compounds with LibDock score of ≥131.581 (based on the LibDock score of control molecules Dinaciclib[99] and RO-3306)[100] were selected for further docking studies along with the screened compounds of DrugBank and Selleckchem. The CDOCKER protocol as used for redocking of co-crystallized ligands was utilized to study the interactions of selected compounds with the binding site residues of CDK1.[101] Hits generated with better C-DOCKER scores as compared to Dinaciclib (a known CDK1/2/5/9 inhibitor) were selected for ligand-protein 2D interaction analysis. These hits were also docked in the binding site of CDK6 for cross-validation during interaction analysis. Each hit was critically analyzed for interactions with key residues of the CDK1 and CDK6 binding sites. Only those compounds that showed key residue interactions with CDK1 and not CDK6 were selected to ensure selective binding. The selected in-house library of compounds was also docked in the binding site of CDK1 (PDB ID: 5LQF) using C-DOCKER protocol; the interactions of the docked pose were analyzed and two hits from these were taken ahead based on the previous study[51] and our analysis.

2.8. Molecular Dynamics (MD) Simulation Studies. To study the stability and the pharmacodynamic behavior of the protein−ligand complexes in the body microenvironment, the selected top ten hits docked with CDK1 showing specific interactions and the two compounds from the in-house library were used as inputs for MD simulation studies along with the controls as detailed earlier.[102] The study was performed using GROMACS 2019.2[52] with GROMOS96 43a1 forcefield starting with the formation of protein topology. The ligand topology was built using the PRODRG server.[103] The protein−ligand complexes were placed in a cubic box for solvation at an equidistant distance of 1 nm from the box edges. The system was then neutralized by the addition of sodium/chloride ions. The hydrogen atoms were constrained using the LINC algorithm[104] and long-range electrostatic computations were done by the particle mesh Ewald (PME) method. Following this, the complexes were energy minimized to clear the steric hindrances between atoms by applying the steepest descent algorithm for 50000 steps. The complexes were then equilibrated under *NVT* and *NPT* simulation ensembles at a constant pressure of 1 atm and temperature of 300 K for 100 ps. Finally, a 100 ns MD simulation was run for each complex, and the potential energy, root-mean-square deviation (RMSD), root-mean-square fluctuation (RMSF), the radius of gyration (RoG), and hydrogen bonds of the resulting trajectories were analyzed using PyMOL and XmGrace software.

2.9. Binding Free Energy Calculations and Molecular Similarity Evaluation. Results from the MD simulation studies were revalidated by evaluating the binding free energies of the complexes by the Molecular mechanics Poisson−Boltzmann surface area (MM-PBSA) method using the g_mmpbsa tool of GROMACS.[105] We calculated the energies from the last stable 20 ns of each MD simulation run keeping all parameters at default based on the following equations as enumerated previously.[106]

$$\Delta G_{\text{bind}} = G_{\text{complex}} - [G_{\text{protein}} + G_{\text{ligand}}] \quad (1)$$

$$G_{(\text{complex/protein/ligand})} = E_{\text{vdw}} + E_{\text{ele}} + G_{\text{sol-pb}} + \gamma\text{SASA} + b \quad (2)$$

The MM-PBSA calculations also include energy components, and the individual energy contributions of the residues were calculated.

Tanimoto Similarity index is the measure of the chemical features that are common to two molecules in comparison. This index has also been regarded as a better choice for fingerprint-based similarity studies.[107] All the final 12 hits were evaluated for their molecular similarity with the control, RO-3306 by means of the Tanimoto similarity index using the "Molecular Similarity Search Tool" in DS 2021.

2.10. Kinase Assay for Potential CDK1 Inhibitors. Finally, the top eight molecules selected on the basis of molecular docking and detailed interaction analysis followed by MD simulations and binding energies and the two in-house library compounds along with control molecules Dinaciclib and RO-3306 were evaluated further using CDK1 kinase assay. The three selected DrugBank hits and RO-3306 were purchased from Cayman Chemical (USA); Dinaciclib was purchased from AdooQ Bioscience USA. The selected five Otava compounds were purchased from Otava Chemicals Ltd. sourced through Molport.com and two compounds were picked from the in-house library[51] for an *in vitro* CDK1 kinase assay performed using the ADP-Glo Kinase Assay from Promega (V6930, V2961) which is a luminescence-based assay where ADP generated from a kinase reaction is estimated by the luminescence signal correlating with the enzyme activity.[108−111] This assay was performed in two steps: First, all the test compounds along with the known inhibitors (Dinaciclib and RO-3306) were tested at fixed concentrations of 10 and 100 μM each; second, the compounds showing ≥50% inhibitory activity at 10 μM were selected for a seven-point dose−response curve starting from 50 μM and diluted up to 0.001 μM. The assay was performed according to the manufacturer's protocol. Briefly, 1 ng of CDK1 protein, 0.2 μg/μL histone H1 substrate, and 50 μM ultrapure ATP were prepared in Kinase Buffer (40 mM Tris pH 7.5; 20 mM $MgCl_2$; 0.1 mg/mL BSA; 50 μM DTT). The test compounds along with the known inhibitors were prepared at the desired concentrations in the kinase buffer. The assay was performed in 384 well white plates from Greiner Bio-One with a reaction volume of 5 μL each where 1 μL of compound was mixed with 2 μL of CDK1 solution (Kinase Buffer in the case of no-

https://doi.org/10.1021/acsomega.4c05414
ACS Omega 2024, 9, 39873−39892

Table 1. Statistical Parameters of the Ten Pharmacophore Models Generated by HypoGen for CDK1 and CDK4/6[a]

A) Ten hypotheses generated for CDK1 by the HypoGen algorithm[b]					
Hypothesis	Total cost	Cost Difference[c]	RMSD (Å)	Correlation	Features
Hypo1_CDK1	150.009	109.56	0.792	0.958	HBA, HBA, HBA, HY
2	153.744	105.83	0.929	0.942	HBA, HBA, HBA, HY
3	154.8	104.77	0.961	0.938	HBA, HBA, HBA, HY
4	156.23	103.37	0.995	0.933	HBA, HBA, HBA, HY
5	157.11	102.45	1.015	0.93	HBA, HBA, HBA, HY
6	157.401	102.17	1.033	0.927	HBA, HBA, HBA, HY
7	157.73	101.84	0.92	0.945	HBA, HBA, HY
8	158.28	101.29	1.056	0.924	HBA, HBA, HBA, HY
9	158.66	100.91	1.067	0.923	HBA, HBA, HBA, HY
10	159.27	100.29	1.082	0.92	HBA, HBA, HBA, HY
B) Ten hypotheses generated for CDK4/6 by the HypoGen algorithm[d]					
Hypothesis	Total cost	Cost Difference[c]	RMSD (Å)	Correlation	Features
Hypo1_CDK4/6	236.98	330.021	0.815	0.972	HBA, HBD, HY, PosIon
2	247.09	319.911	0.987	0.959	HBA, HBD, HY, PosIon
3	256.06	310.941	1.168	0.942	HBA, HBD, HY, PosIon
4	262.14	304.861	1.245	0.934	HBA, HBD, HY, PosIon
5	264.08	302.921	1.27	0.931	HBA, HBD, HY, PosIon
6	270.54	296.461	1.342	0.922	HBA, HBD, HY, PosIon
7	272.87	294.131	1.379	0.918	HBA, HBD, HY, PosIon
8	273.09	293.911	1.371	0.919	HBA, HBD, HY, PosIon
9	273.2	293.801	1.374	0.919	HBA, HBD, HY, PosIon
10	274.46	292.541	1.382	0.918	HBA, HBD, HY, PosIon

[a]HBA − hydrogen bond acceptor, HBD − hydrogen bond donor, HY − hydrophobic, PosIon − positive ionizable. [b]Fixed cost = 138.161, Null cost = 259.573, Configuration cost = 15.94 (all costs are measured in bits). [c]Difference between the null cost and the total cost. [d]Fixed cost = 215.523, Null cost = 567.001, Configuration cost = 12.58 (all costs are measured in bits).

enzyme control) and 2 μL of ATP/Substrate mixture solution for 60 min. After incubation, 5 μL of ADP Glo Reagent was added to all the wells to end the kinase reaction. This step was followed by 40 min of incubation. Finally, 10 μL of Kinase Detection Buffer was added to all the wells and incubated for 60 min in the dark to convert ADP to ATP and quantify the light generated using a luciferase/luciferin reaction. The percentage enzyme activity was determined by using the following formula:

$$\%\ \text{Enzyme Activity} = \frac{(\text{Test sample} - \text{no enzyme control})}{(\text{Enzyme control} - \text{no enzyme control})} \times 100 \quad (3)$$

where the test samples were the test compounds at varying concentrations along with substrate and enzyme and enzyme control was without any compounds.

3. RESULTS

3.1. Generation of Pharmacophores. A total of 10 3D-QSAR pharmacophore models were generated for CDK1 from the training set of molecules. All the statistical parameters related to the 10 hypotheses are listed in Table 1A. Out of the 10 hypotheses, Hypo1_CDK1 was selected as the best predictive model with the highest cost difference, highest correlation and lowest RMSD value. Hypo1_CDK1 consists of three HBA and one HY feature, a correlation coefficient of 0.958, an RMSD value of 0.792, and a cost difference of 109.56 indicating a good model for activity prediction. The experimental and predicted activity of training set compounds of CDK1 based on Hypo1_CDK1 are enumerated in Table S1. Highly active (+++), moderately active (++), and least active (+) were predicted by the algorithm based on the activity of <60 nM, 60−1000 nM, and >1000 nM respectively. As shown in Figure 1A, most active compound **1** maps to all the essential features (3 HBA, 1 HY) of Hypo1_CDK1, moderately active compound **17** maps to 3 essential features (2 HBA, 1 HY), and least active compound **35** maps to only 2 features (2 HBA). From the mapping patterns, we can infer that the presence of hydrophobic groups is necessary for a strong interaction with the binding site residues.

Next, a total of 10 pharmacophores were built for CDK4/6 from the training set of 60 CDK4/6 inhibitors to validate the accuracy and effectiveness of the CDK1 pharmacophore (Table 1B). Hypo1_CDK4/6 with one HBD, one HBA, one HY, and one PosIon feature characterized by the highest correlation of 0.972, low RMSD value of 0.815 and highest cost difference of 330.021 was selected as the CDK4/6 prediction model. The presence of all four features is critical to achieving CDK4/6 selectivity. The experimental and predicted activities of the training set molecules are listed in Table S3.

Active compounds (+++), moderately active (++), and least active (+) were predicted based on the activity of ≤20 nM, >20 nM but ≤1000 nM, and >1000 nM, respectively. Compounds in the CDK4/6 training set were also mapped to the generated model, and a representation of the same is shown in Figure S3A with the highly active Compound **1′** (maps to all four features), moderately active compound **25′** (maps to HBA, HY, PosIon excluding HBD), and least active compound **59′** (maps to only HY and PosIon). The feature sets for CDK1 and CDK4/6 training sets were different for the respective models generated showcasing subtype selectivity.

3.2. Validation of Generated Pharmacophores. *3.2.1. Cost Function Analysis.* Certain costs are generated

https://doi.org/10.1021/acsomega.4c05414
ACS Omega 2024, 9, 39873−39892

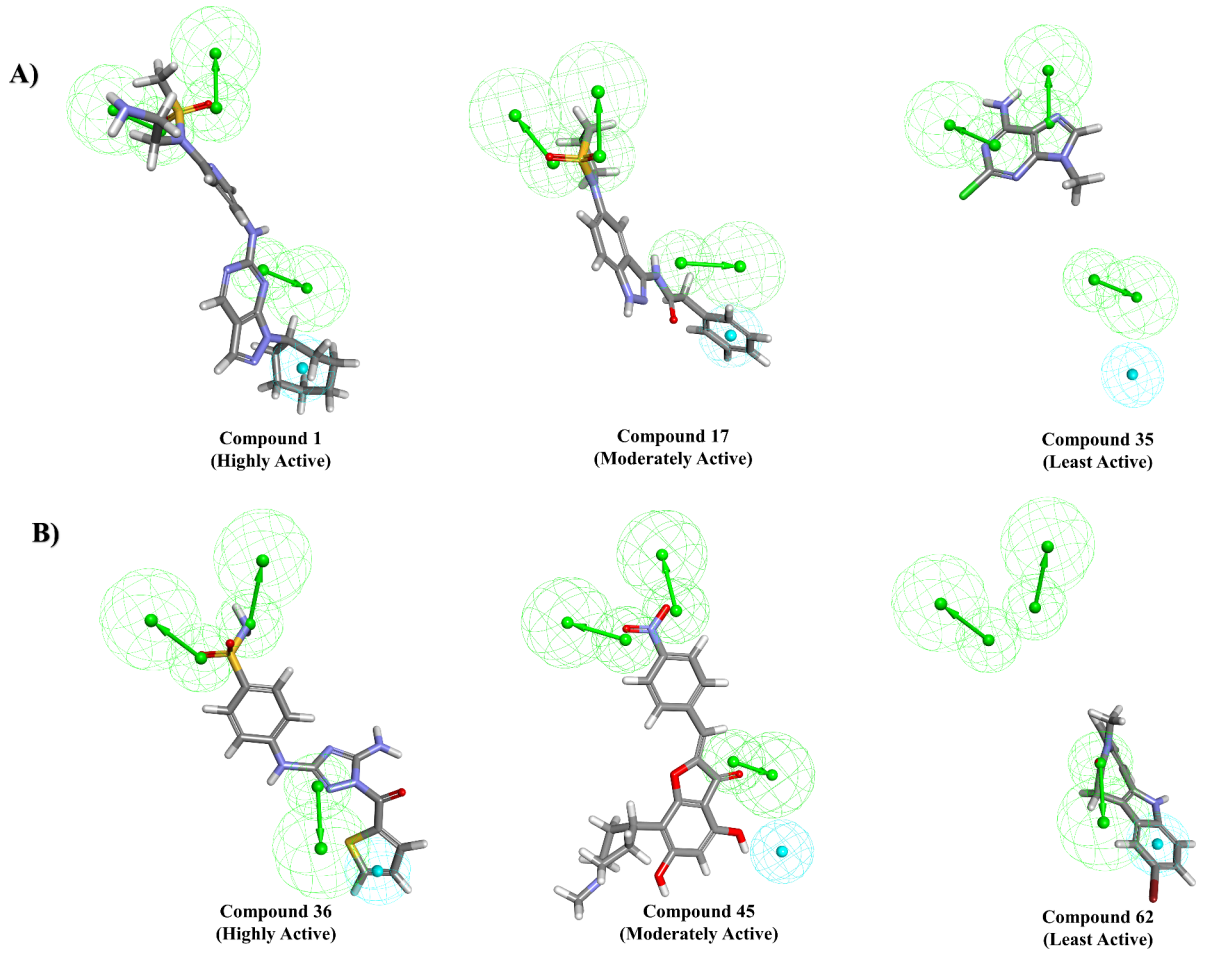

Figure 1. Mapping results of the A) training set and B) test set compounds with the CDK1 pharmacophore (Hypo1_CDK1). Hypothesis features are color-coded as HBA - light green and HY -cyan.

by the HypoGen algorithm to determine the statistical significance during pharmacophore development. In the case of CDK1, the fixed cost was calculated to be 138.161, the null cost was 259.573, and the cost difference (null cost − total cost) for Hypo1_CDK1 was 109.56 which is greater than 100 bits indicating that the model was not developed by chance and has good more than 90% positive prediction ability. The configuration cost for Hypo1_CDK1 was 15.94 which is less than 17 as required indicating low complexity of the generated pharmacophore. For CDK4/6, the fixed cost was 215.523, the null cost was 567.001, and the cost difference for Hypo1_CDK4/6 was 330.021. Here, the configuration cost was also satisfied at 12.58, indicating the model Hypo1_CDK4/6 for CDK4/6 is a good prediction model to cross-validate the hits screened out by CDK1 pharmacophore.

3.2.2. Fischer Randomization Method. To analyze whether a true correlation exists between the structures and activity data, 19 random spreadsheets were generated for each training set at a 95% confidence interval. When compared to CDK1 pharmacophore and CDK4/6 pharmacophore in Figure 2 and Figure S4 respectively, the cost values of the random data were higher and the correlations were lower suggesting that the pharmacophores generated from the training sets are truly correlating the structures with their activity data. These results show that Hypo1_CDK1 for CDK1 and Hypo1_CDK4/6 for CDK4/6 are the best that may be used as a 3D query to screen potential hits from compound libraries and databases.

3.2.3. Internal and External Validation Using the Training Set and Test Set. A pharmacophore can be considered a good prediction model if it can correctly predict the activity of a set of molecules. To this effect, regression analysis was performed for the training set as well as an external test set of different compounds with known activity in the case of both CDK1 and CDK4/6. As shown in Figure S1 and S2, R^2 was equal to 0.9218 (training set) and 0.8131 (test set) for Hypo1_CDK1 and 0.95 (training set) and 0.9456 (test set) for Hypo1_CDK4/6. The predicted and experimental activities of the test set compounds of CDK1 are listed in Table S2. Active compounds of the test set were predicted as highly active, except for compounds **41** and **44** which were predicted as moderately active. All of the moderately active compounds were predicted as such except compounds **46** and **49** which were overestimated as active. All the inactive compounds were predicted as inactive except compounds **57** and **59** which were overestimated as moderately active. Overestimation of the compounds can be attributed to their conformational flexibility, whereas the underestimation may be due to the conformational rigidness of the compounds.

Similarly, the predicted and experimental activities of the test set compounds of CDK4/6 are listed in Table S4. All the active, moderately active, and inactive compounds were predicted correctly.

Like the training set molecules, test set compounds were also mapped to the pharmacophores generated. In the test set

https://doi.org/10.1021/acsomega.4c05414
ACS Omega 2024, 9, 39873−39892

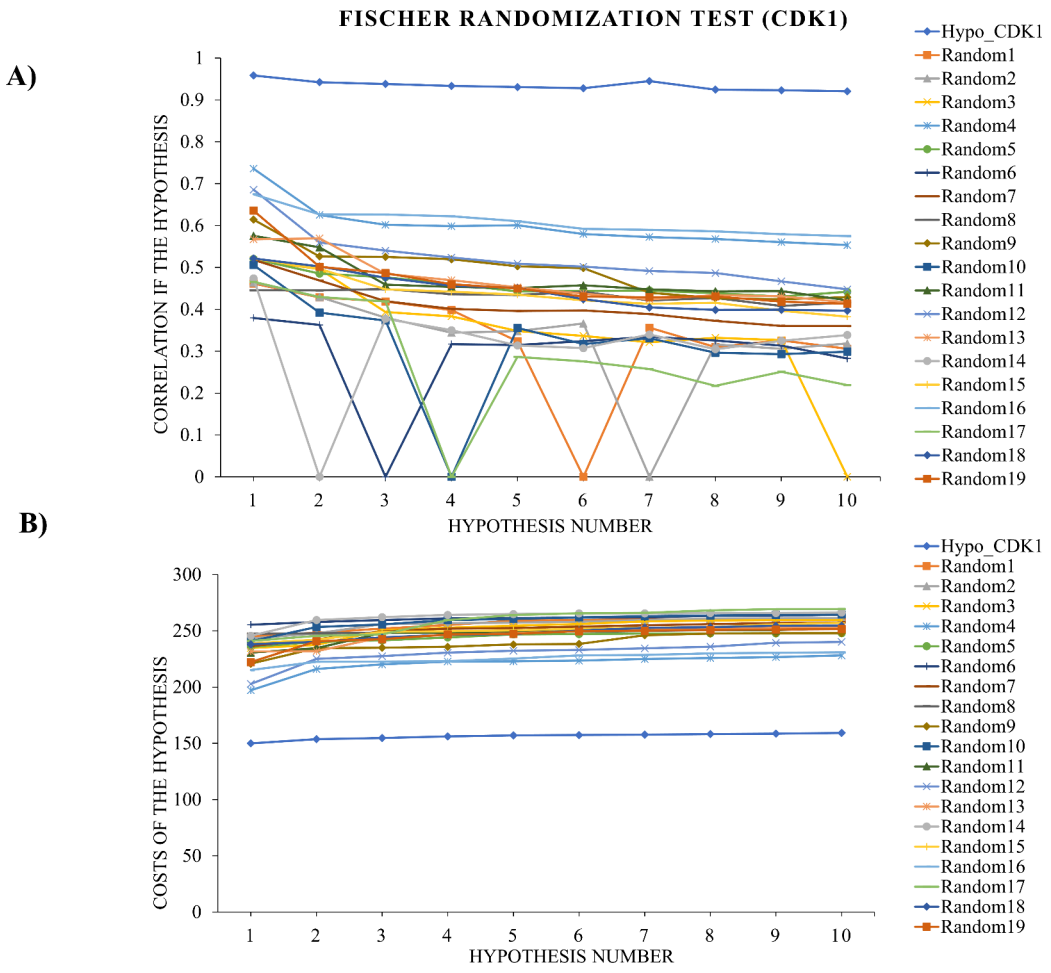

Figure 2. Fischer cross-validation test for Hypo1_CDK1. A) Comparison of correlation of Hypo1_CDK1 with other hypotheses obtained after randomization. B) Comparison of costs of our pharmacophore (Hypo1_CDK1) with other hypotheses.

of CDK1, highly active compound **36** mapped to all four features of the model, moderately active compound **45** mapped to three HBA features, and least active compound **62** mapped to only two features, one HBA and one HY (Figure 1B). In the test set of CDK4/6, highly active compound **60′** mapped to all four features, moderately active compound **77′** mapped to three features (one HBA, one HBD, and one HY), and least active compound **105′** mapped to only two features (one HBD and one HY, Figure S3B). Mapping results of the test sets again infer that all four features should be present in a compound to be highly active for the respective target proteins.

3.3. Virtual Screening and Filtration of Initial Hits. The validated best pharmacophore model for CDK1 and CDK4/6 was used to screen 2,88,671 compounds of DrugBank, Selleckchem databases (Kinase Inhibitors, Natural Products), and Otava libraries (Kinase targeted, Lead-like, and Drug-like green collection compounds) for potential hits as CDK1 inhibitors. A total of 12,205 compounds mapping to all four features of the CDK1 model with fit value ≥6.39 in comparison to the control ligands Dinaciclib and RO-3306 were selected as primary hits. These compounds had an estimated IC_{50} of <30 nM for CDK1. To screen CDK1 selective molecules, all compounds from each database were also screened using Hypo1_CDK4/6. The compounds with fit values of ≥8.9 (based on fit values of CDK4/6 selective inhibitors, Ribociclib, Palbociclib, and Abemaciclib) and common in both screenings were carefully examined and removed from the primary hit list generated for CDK1. Only those hits were selected which were estimated to be highly active for CDK1 and not CDK4/6. A series of 15 compounds from the in-house library of 1,3,4-oxadiazole thiones[51] was also mapped to Hypo1_CDK1 and Hypo1_CDK4/6. Compounds that mapped to all four features of Hypo1_CDK1 and not to the features of Hypo1_CDK4/6 were selected for further analysis. These 12,210 hits were then filtered according to their drug-likeness, pharmacokinetic, and pharmacodynamic properties using the Lipinski rule of five, Veber rule, and ADMET and TOPKAT tools of DS 2021. Finally, 311 hits from DrugBank (DB) and Selleckchem (SC) libraries, 9,994 hits from Otava Libraries and 5 hits from the in-house library were selected for docking studies (Figure S5).

3.4. Molecular Docking Studies. The co-crystallized ligands were redocked in the determined binding sites of CDK1 (5LQF) and CDK6 (5L2T) using the C−Docker tool of DS 2021. After redocking, the RMSD values of PDB ligands were 0.46 Å for 5LQF and 0.98 Å for 5L2T, respectively. As the RMSD obtained was below 2 Å, it was concluded that the redocked pose superimposes well with the PDB structure (Figures S6A and S9A). Therefore, the same protocol was used for docking studies using C-DOCKER. Due to the presence of a large data set after the filtration step, Otava library compounds (9,994) were first subjected to a fast docking-based filtration step using the LibDock module of Discovery Studio, narrowing down to a better selection of hits for the C-

https://doi.org/10.1021/acsomega.4c05414
ACS Omega 2024, 9, 39873−39892

Table 2. DrugBank, Selleckchem, Otava Databases' and In-House Library Compounds Retrieved from Virtual Screening with Their Estimated Activity, Fit Value, ADMET Profile, Toxicity and Docking Scores along with CDK1 and pan CDK Inhibitors Docked with 5LQF[a]

Compound No.	Compound Code	Fit Value (bits)	Estimated Activity (nM)	ADMET Status	Ames Mutagenicity	−(C-Docker Score)	−(C-Docker Int. Energy)
DB_1	**DB09299**	**7.11**	**16.5737**	**Passed**	**Non-Mutagen**	**56.669**	**58.4452**
DB_2	**DB12896**	**7.67**	**4.51634**	**Passed**	**Non-Mutagen**	**53.8846**	**50.6598**
DB_3	DB15268	7.16	14.66	Passed	Non-Mutagen	53.8356	56.1652
DB_4	DB06368	7.83	3.13436	Passed	Non-Mutagen	51.668	60.461
DB_5	DB00775	7.46	7.41686	Passed	Non-Mutagen	51.076	58.1274
DB_6	**DB06536**	**7.87**	**2.8322**	**Passed**	**Non-Mutagen**	**50.7837**	**58.032**
DB_7	**DB15106**	**7.19**	**13.5353**	**Passed**	**Non-Mutagen**	**49.3642**	**56.5197**
DB_8	DB12795	7.08	17.7159	Passed	Non-Mutagen	49.3281	52.8957
DB_9	DB05478	7.1	16.8163	Passed	Non-Mutagen	48.8431	50.5858
DB_10	DB12022	6.89	27.1139	Passed	Non-Mutagen	46.9111	53.453
DB_11	**DB15059**	**7.11**	**16.5844**	**Passed**	**Non-Mutagen**	**46.8739**	**55.5356**
DB_12	DB13091	7.74	3.83427	Passed	Non-Mutagen	46.8016	63.9165
DB_13	DB13115	7.32	10.1734	Passed	Non-Mutagen	46.205	55.1937
DB_14	DB11433	7.6	5.36923	Passed	Non-Mutagen	45.2041	53.7037
DB_15	DB12376	7.01	20.7923	Passed	Non-Mutagen	44.671	59.8535
SC_1	S3917	8.07	1.78341	Passed	Non-Mutagen	48.8864	50.0674
SC_2	S0391	7.11	16.3418	Passed	Non-Mutagen	46.3671	60.9872
SC_3	S2692	7.01	20.5479	Passed	Non-Mutagen	46.2687	60.0086
OT_1	**6241970**	**7.22**	**13.0364**	**Passed**	**Non-Mutagen**	**57.8153**	**57.9864**
OT_2	**1098939**	**6.91**	**26.4793**	**Passed**	**Non-Mutagen**	**56.2028**	**58.9052**
OT_3	6138328	7.74	3.85711	Passed	Non-Mutagen	56.0085	49.7617
OT_4	1158149	7.31	10.5129	Passed	Non-Mutagen	53.5061	55.7603
OT_5	6237079	7.37	9.1761	Passed	Non-Mutagen	51.6334	60.7038
OT_6	1158701	6.99	21.4435	Passed	Non-Mutagen	51.5977	54.8314
OT_7	1108850	7.23	12.5906	Passed	Non-Mutagen	50.9011	56.7126
OT_8	**7011940372**	**7.68**	**4.48338**	**Passed**	**Non-Mutagen**	**50.8829**	**60.8282**
OT_9	2190452	6.94	24.6202	Passed	Non-Mutagen	50.6193	52.2701
OT_10	6240949	6.92	25.5173	Passed	Non-Mutagen	50.5385	52.2416
OT_11	**11184881**	**7.02**	**20.2222**	**Passed**	**Non-Mutagen**	**49.884**	**55.8819**
OT_12	11184860	7.01	21.0361	Passed	Non-Mutagen	49.0933	51.1992
OT_13	1303168	7.18	13.9765	Passed	Non-Mutagen	48.5074	52.1073
OT_14	2190450	7.03	19.8989	Passed	Non-Mutagen	48.4833	50.6536
OT_15	6239985	6.95	24.1166	Passed	Non-Mutagen	48.4012	56.1803
OT_16	6667482	7.73	3.9446	Passed	Non-Mutagen	48.2042	54.0588
OT_17	**6242917**	**7.22**	**13.0174**	**Passed**	**Non-Mutagen**	**48.1384**	**57.9874**
OT_18	6237386	7.59	5.4456	Passed	Non-Mutagen	47.4376	50.5838
OT_19	6244399	7.21	13.1637	Passed	Non-Mutagen	47.3641	55.2094
OT_20	6237835	6.90	26.6269	Passed	Non-Mutagen	47.2906	54.9457
OT_21	6236879	7.21	13.1283	Passed	Non-Mutagen	47.1324	51.283
OT_22	6237291	7.03	19.7522	Passed	Non-Mutagen	46.7737	57.4466
OT_23	1108847	7.23	12.5091	Passed	Non-Mutagen	46.695	50.6122
OT_24	2190444	7.31	10.4014	Passed	Non-Mutagen	46.0911	48.7303
OT_25	11184509	7.22	12.8252	Passed	Non-Mutagen	45.5757	55.5997
OT_26	1098706	7.18	14.2035	Passed	Non-Mutagen	45.5599	56.9944
OT_27	1159063	7.17	14.536	Passed	Non-Mutagen	45.5509	47.9741
OT_28	1107936	6.99	22.0698	Passed	Non-Mutagen	45.4111	57.8151
OT_29	1108848	8.29	1.09265	Passed	Non-Mutagen	45.3514	48.7671
OT_30	1158709	8.36	0.94245	Passed	Non-Mutagen	45.2624	51.6488
OT_31	1115049	8.53	0.6316	Passed	Non-Mutagen	45.2566	54.9132
OT_32	3461212	6.92	25.9717	Passed	Non-Mutagen	45.0681	52.93
OT_33	1182485	7.35	9.62502	Passed	Non-Mutagen	45.0482	71.906
OT_34	6237732	7.67	4.54939	Passed	Non-Mutagen	44.9024	58.6972
OT_35	1090498	7.25	11.8945	Passed	Non-Mutagen	44.2326	51.8795
IH_9	**3i**	**8.13**	**1.6**	**Passed**	**Non-Mutagen**	**6.38042**	**47.0856**
IH_10	**3j**	**4.62**	**5100**	**Passed**	**Non-Mutagen**	**8.80407**	**44.8614**
	NU6102	*8.79*	*0.348253*	*Passed*	*Non-Mutagen*	*44.378*	*56.8975*
	Dinaciclib	*7.57*	*5.76127*	*Passed*	*Non-Mutagen*	*44.1526*	*55.0005*
	CGP74514A	*6.39*	*87.7965*	*Passed*	*Non-Mutagen*	*41.0935*	*51.9025*

https://doi.org/10.1021/acsomega.4c05414
ACS Omega 2024, 9, 39873−39892

Table 2. continued

Compound No.	Compound Code	Fit Value (bits)	Estimated Activity (nM)	ADMET Status	Ames Mutagenicity	−(C-Docker Score)	−(C-Docker Int. Energy)
	AZD5438	*6.39*	*87.7965*	*Passed*	*Non-Mutagen*	*33.6356*	*44.7108*
	RO-3306	*6.39*	*87.7965*	*Passed*	*Non-Mutagen*	*11.1971*	*43.9489*

[a]Compounds in **bold** were selected based on C-Docker scores and 2D interaction analysis with both CDK1 and CDK6.

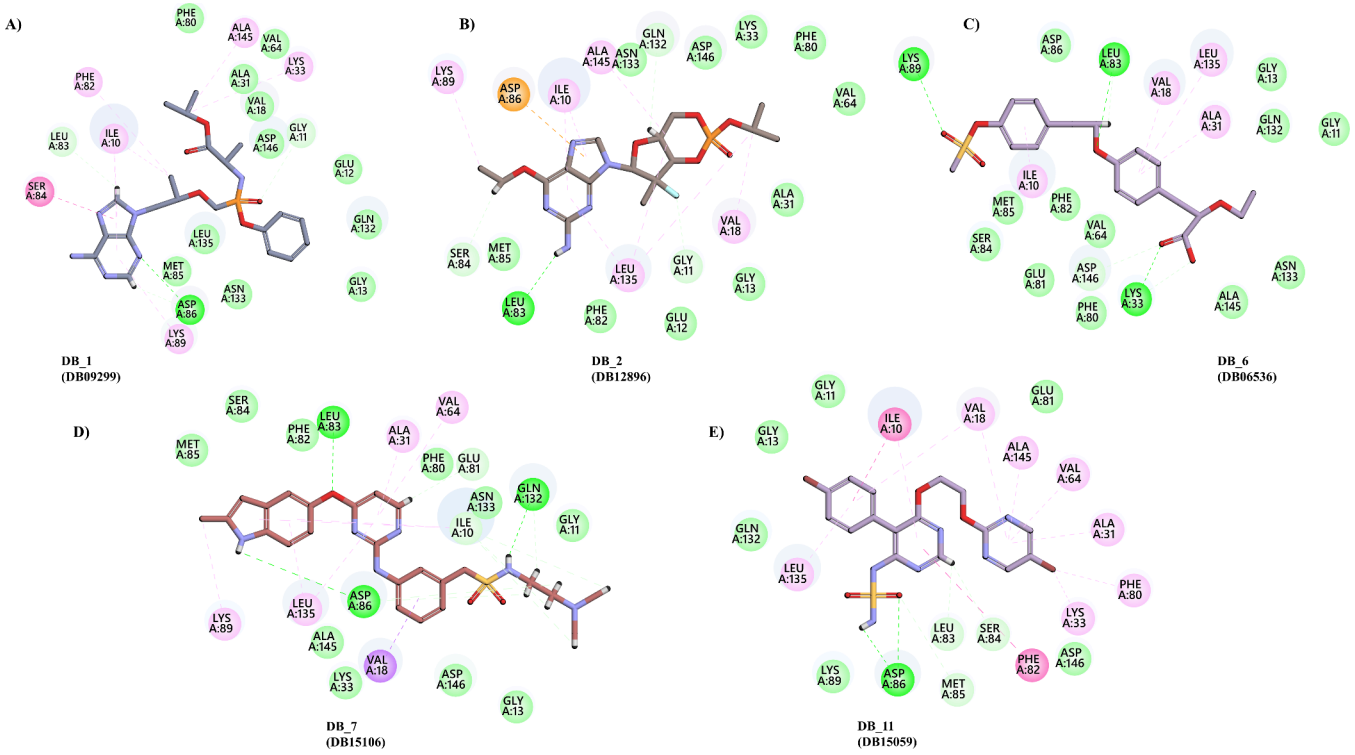

Figure 3. 2D interactions of the selected 5 DrugBank hits A) **DB_1 (DB09299)**, B) **DB_2 (DB12896)**, C) **DB_6 (DB06536)**, D) **DB_7 (DB15106)**, and E) **DB_11 (DB15059)** docked in the binding site of 5LQF.

DOCKER protocol. Compounds having a LibDock score >131.581 were selected based on the LibDock score of Dinaciclib and RO-3306. A total of 618 compounds (311 from DB (245), SC (66)), 307 from Otava library) were then docked in the binding site of CDK1 using the C-DOCKER tool in DS 2021. A total of 10 poses were generated for each docked compound. Based on the −(C-Docker scores), the best poses of 53 hits (15 from DB, 3 from SC, 35 from Otava) with a score better than that of the control ligand Dinaciclib (44.15 kcal/mol) were selected for the 2D interaction analysis. The five selected compounds from the in-house library were also docked in the binding site of CDK1; their C-Docker scores were calculated and 2D interaction maps were studied. Based on these parameters and their impact on cell cycle proteins as shown in the previous study,[51] two of these compounds were taken further for MD simulation studies (Table 2).

3.4.1. Interaction of Ligands within the CDK1 Binding Site. Recent studies[11,92] showed that the active site of CDK1 consisted of certain key residues. These were Ile10, Gly11, Glu12, Gly13, Val18, Ala31, Lys33, Val64, Phe80, Glu81, Phe82, Leu83, Ser84, Met85, Asp86, Lys89, Gln132, Asn133, Leu135, and Asp146. When the co-crystallized ligand NU6102 interacted with the CDK1 (5LQF) active site, the purine moiety formed hydrogen bonds with Glu81 and Leu83. The sulfonamide group formed a hydrogen bond with Asp86. It formed hydrophobic interactions with Ile10, Val18, Ala31, Val64, Phe82, and Leu135. NU6102 exhibited van der Waals interactions with Gly11, Glu12, Gly13, Phe80, Ser84, Met85, Lys89, Gln132, Asn133, and Asp146 (Figure S6B). Other known inhibitors of CDK1, namely, Dinaciclib and RO-3306, were also docked to the binding site to assess the most important and selective interactions with CDK1. Dinaciclib, a CDK1/2/5/9 inhibitor, when docked to CDK1 formed hydrogen bond interactions through the purine moiety with Leu83. It is hydroxyethylpiperidine group formed hydrogen bonds with Ile10 and Asp86. The core formed hydrophobic interactions with Ile10, Val18, Ala31, Phe80, and Leu135. In addition, the pyridine oxide group formed a pi-alkyl bond with Ile10. It also formed van der Waals interactions with Gly11, Glu12, Gly13, Lys33, Val64, Glu81, Phe82, Ser84, Met85, Lys89, Gln132, Asn133, Ala145, and Asp146 (Figure S7A). Finally, when RO-3306, a CDK1-specific inhibitor, was docked; it interacted through its thiazolone amino group, forming a hydrogen bond with Asp86. The quinoline group formed major hydrophobic interactions with Val18, Ala31, Lys33, Val64, Phe80, Met85, and Ala145, while the thienyl group formed a pi-alkyl bond with Ile10 and a pi-σ bond with Met85. There were eight van der Waals interactions with Gly11, Glu81, Phe82, Ser84, Lys89, Gln132, Leu135, and Asp146 (Figure S7B).

To check specific and distinct interacting residues in the CDK4/6 binding site, the co-crystallized ligand, Ribociclib was

https://doi.org/10.1021/acsomega.4c05414
ACS Omega 2024, 9, 39873−39892

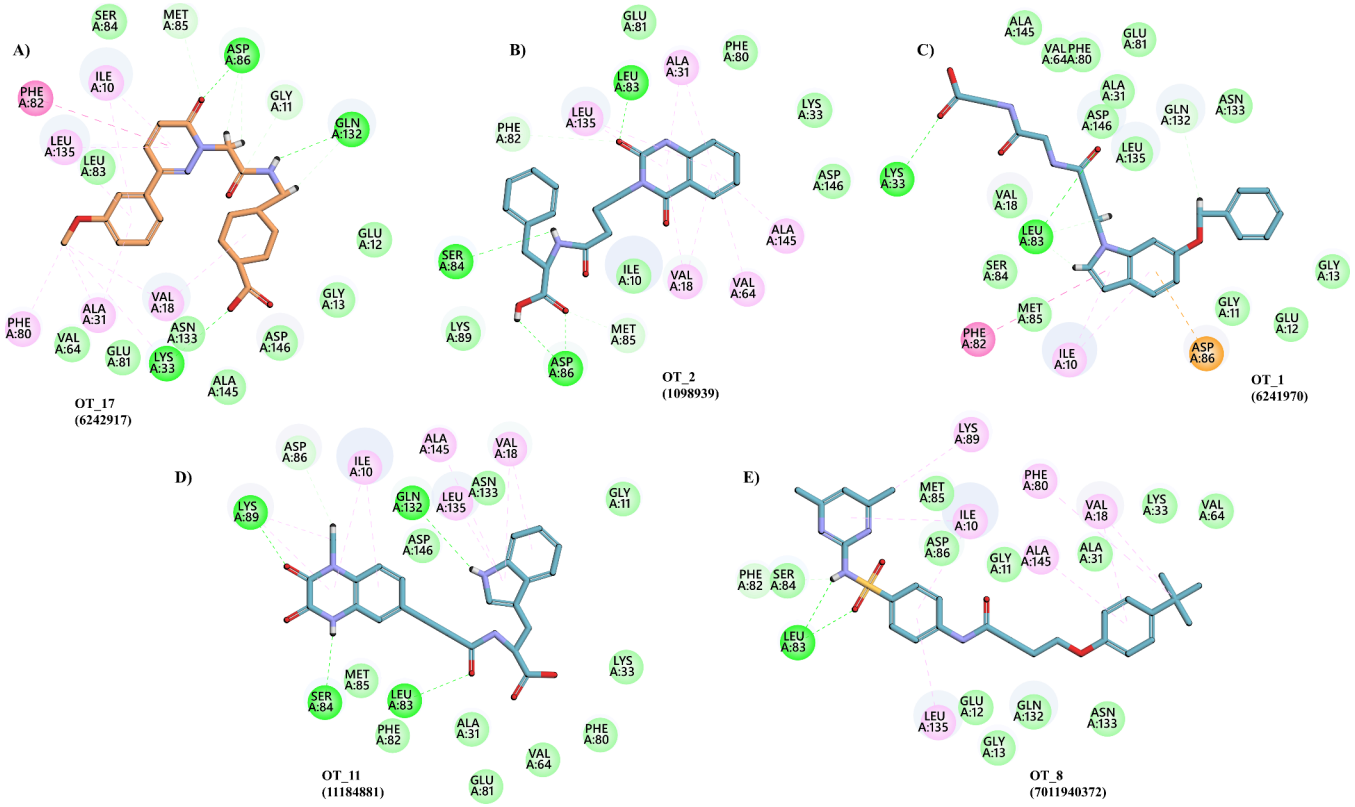

Figure 4. 2D interactions of the selected 5 Otava library hits A) **OT_17 (6242917)**, B) **OT_2 (1098939)**, C) **OT_1 (6241970)**, D) **OT_11 (11184881)**, and E) **OT_8 (7011940372)** docked in the binding site of 5LQF.

also redocked to CDK6 (5L2T), and key interactions were observed (Figure S9B). According to the previous reports,[112,113] a hydrogen bond with Val101 and a strong hydrophobic interaction with His100 determines CDK4/6 selectivity for a compound. Correspondingly, in the CDK1 binding site, Leu83 and Phe82 serve analogous roles as key residues. These residues are crucial for CDK1's active site. Therefore, 53 selected hits based on C-Docker scores were visually inspected for interactions with CDK1 key residues (Phe82, Leu83, Ser84, Met85 and Asp86), which played a crucial role in the activity of CDK1. Next, the compounds were docked into the binding site of CDK6 to assess their formation of hydrogen bonds with Val101 and hydrophobic interactions with His100. To ensure selectivity against CDK1, compounds lacking these interactions, which are pivotal for CDK6 activity, were filtered out. Based on this selection criteria, five hits from DrugBank and five from the Otava libraries were finalized for future protocols. These top selected ten hits showed all of the important key residue interactions with CDK1. The corresponding poses of the selected compounds when docked to CDK6 did not show any significant interaction with its key residues.

The purine ring of **DB_1 (DB09299)** established hydrogen bonds with Leu83 and Asp86. The oxygen of the phosphoryl group of DB_1 formed a hydrogen bond with Gly11. The purine ring also formed hydrophobic interactions with Ile10, Ser84, and Lys89. The methyl side chain of the propanoyl moiety formed alkyl bonds with Ile10 and Phe82. There were alkyl hydrophobic bonds between the isopropyl group and Lys33 and Ala145. It also showed van der Waals interactions with Glu12, Gly13, Val18, Ala31, Val64, Phe80, Met85, Gln132, Asn133, Leu135, and Asp146 (Figure 3A).

DB_2 (DB12896) through an amino group on the purine moiety built conventional hydrogen bonds with Leu83 and a carbon−hydrogen bond with Ser84 through the CH_2 group of the ethoxy side chain. It showed hydrophobic interactions with Ile10, a pi-anion bond with Asp86, an alkyl bond with Lys89 and a pi-alkyl bond with Leu135. The compound formed two more carbon−hydrogen bonds with Gly11 through fluorine and another with Gln132 through the H atom of the dioxo phosphinine ring. It formed hydrophobic interactions with Val18, Leu135 and Ala145. van der Waals interactions with Glu12, Gly13, Ala31, Lys33, Val64, Phe80, Phe82, Met85, Asn133, and Asp146 (Figure 3B).

DB_6 (DB06536) consisted of a propionic acid group interacting with Lys33 and Asp146 through hydrogen bonds. Hydrogen bonds were also present between the ethoxy group and Leu83; the sulphonyl oxygen was present and Lys89. Pi-alkyl bonds were formed between the Ile10 and phenyl ring-bearing sulfonyl group and with Val18, Ala31 and Leu135 through the phenyl ring at the other end of the molecule toward the catalytic cleft. There were van der Waals interactions with Gly11, Gly13, Val64, Phe80, Glu81, Phe82, Ser84, Met85, Asp86, Glu132, Asn133, and Ala145 (Figure 3C).

DB_7 (DB15106) constituted five hydrogen bonds, with Ile10 through the hydrogen atoms of the dimethyl amino group; with Glu81, Leu83, and Asp86 through hydrogen and oxygen atoms in the indole ring, and with Gln132 through the sulphonamide group. Hydrophobicity was reflected by the aromatic rings present, a pi-alkyl bond with Ile10, pi-σ bond with Val18, pi-alkyl with Ala31, Val64; alkyl bond with Lys89 and a pi-alkyl bond with Leu135. van der Waals interactions

https://doi.org/10.1021/acsomega.4c05414
ACS Omega 2024, 9, 39873−39892

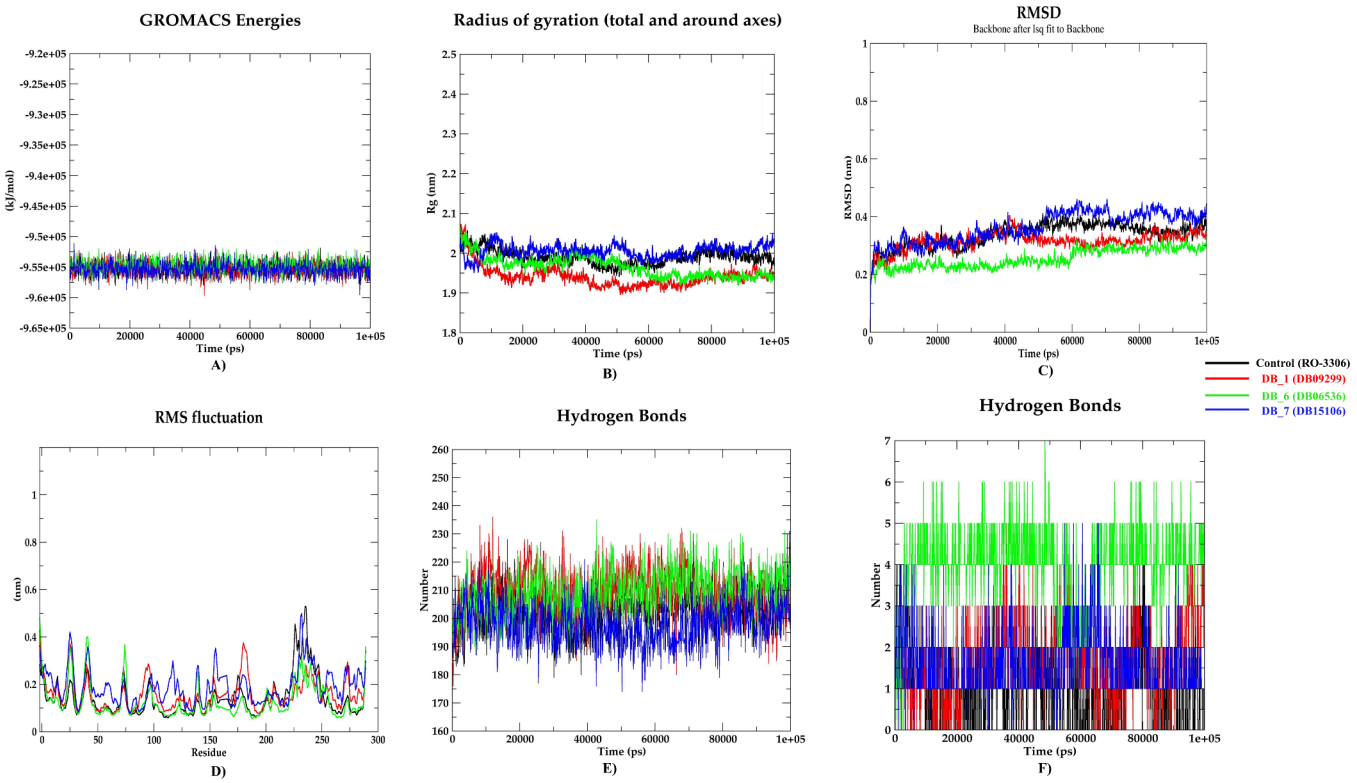

Figure 5. A) Energies, B) radius of gyration, C) RMSD, D) RMSF, E) hydrogen bonds within the protein, and F) hydrogen bonds between the ligands (DrugBank) and protein throughout 100 ns.

were exhibited with Gly11, Gly13, Lys33, Phe80, Phe82, Ser84, Met85, Asn133, Ala145, and Asp146 (Figure 3D).

In the case of **DB_11 (DB15059)**, the sulfamide and its associated pyrimidine ring constituted hydrogen bonds with Leu83, Ser84, Met85, and Asp86; a pi-pi stacked bond with Ile10; amide-pi stacked bond with Phe82; the bromine of the other pyrimidine ring formed alkyl bond with Lys33 and Phe80; pi-alkyl bond with Val18, Ala31, Val64, and Ala145; the bromophenol ring with Leu135 and van der Waals interactions with Gly11, Gly13, Glu81, Lys89, Gln132, and Asp146 (Figure 3E).

The acetyl group, the oxopyridazine group, and the amine amino group attached to the cyclohexane ring in the otava library compound **OT_17 (6,242,917)** formed hydrogen bonds with Gly11, Lys33, Met85, Asp86, and Gln132; the core substituents consisting of the substituted aromatic rings formed alkyl and pi-alkyl bonds with Ile10, Val18, Ala31, Phe80, Phe82, and Leu135. There were nine van der Waals interactions with Glu12, Gly13, Val64, Glu81, Leu83, Ser84, Asn133, Ala145, and Asp146 (Figure 4A).

The quinazoline group of another compound, **OT_2 (1,098,939)** exhibited hydrogen bonds with Phe82 and Leu83; the phenylalanine group with Ser84, Met85, and Asp86. Hydrophobic interactions were formed by the quinazoline aromatic rings with Val18, Ala31, Val64, Leu135 and Ala145 in the catalytic core. There were six van der Waals interactions with Ile10, Lys33, Phe80, Glu81, Lys89, and Asp146 (Figure 4B).

The carbonyl oxygen of the propanoyl group (middle part of the molecule) interacted through a hydrogen bond with Leu83 and the terminal carboxylate of **OT_1 (6,241,970)** with Lys33. It also made a carbon−hydrogen bond with Gln132; it is indole ring formed a pi-alkyl bond with Ile10, a pi-pi stacked bond with Phe82, and a pi-anion bond with Asp86. It also showed van der Waals interactions with Gly11, Glu12, Gly13, Val18, Ala31, Val64, Phe80, Glu81, Ser84, Met85, Asn133, Ala145, and Asp146 (Figure 4C).

OT_11 (11,184,881) indicated hydrogen bond interactions between the propanoyl group and Leu83; the quinoxaline group interacted with Ser84, Asp86 and Lys89; the indole ring interacted with Gln132. Hydrophobic interactions of the indole ring were observed with Ile10, Val18, Leu135, and Ala145 and van der Waals interactions with Gly11, Ala31, Lys33, Val64, Phe80, Glu81, Phe82, Met85, Asn133, and Asp146 (Figure 4D).

The sulfonamide group of **OT_8 (7011940372)** interacted through hydrogen bonds with Phe82 and Leu83. OT_8 also exhibited hydrophobic interactions with Ile10, Val18, Phe80, Lys89, Leu135, and Ala145 through the phenoxy group, the phenyl ring and the pyrimidine ring along with their side chains. It exhibited van der Waals interactions with Gly11, Glu12, Gly13, Ala31, Lys33, Val64, Ser84, Met85, Asp86, Gln132, and Asn133 (Figure 4E). The generic names or codes of these compounds, 2D structures, and types of interactions along with their sources or indications are listed in Table S6.

In the case of in-house library compounds, **IH_9 (3i)** formed hydrogen bonds with Leu83 through its oxadiazole thione moiety. The nitro side chain attached to the phenyl ring in the hinge region formed hydrophobic interactions with Asp86 and Lys89. The oxadiazole ring and the substituted aromatic ring inside the binding pocket made pi-alkyl bonds with Ile10, Val18, Ala31 and Leu135. van der Waals interactions were formed with Ser84, Met85 and Phe82 in the hinge region; with Gly11, Glu12, Gly13, Glu81, Gln132, Asn133, Ala145, and Asp146 in the catalytic cleft (Figure S8A).

https://doi.org/10.1021/acsomega.4c05414
ACS Omega 2024, 9, 39873−39892

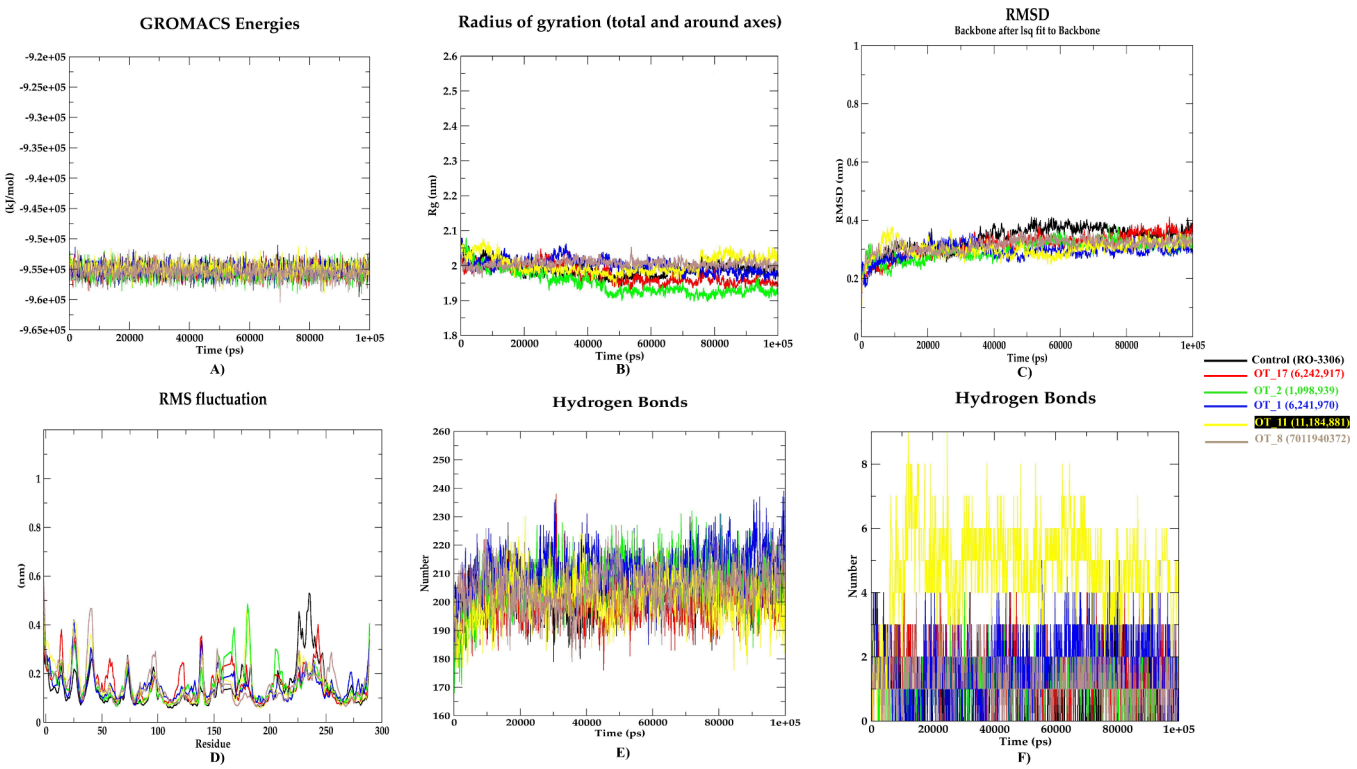

Figure 6. A) Energies, B) radius of gyration, C) RMSD, D) RMSF, E) hydrogen bonds within the protein, and F) hydrogen bonds between the ligands (Otava) and protein throughout 100 ns.

Similar to IH_9, the thione of **IH_10 (3j)** formed a hydrogen bond with Leu83. The aromatic rings formed hydrophobic interactions with Ile10, Val18, Ala31, and Leu135. In this case, as shown in Figure S8B, the fluoride side chain did not interact strongly with residues in the hinge region but formed van der Waals interactions with Phe82, Ser84, Met85, Asp86, and Lys89. The *tert*-butyl phenyl ring exhibited van der Waals interactions with Gly11, Glu12, Gly13, Glu81, Gln132, Asn133, Ala145, and Asp146.

3.5. Molecular Dynamics (MD) Simulation Studies. To validate our findings from HTVS and docking studies, MD simulation studies were performed for the top ten hit compounds and two in-house library compounds **IH_9** and **IH_10** along with the CDK1-specific inhibitor RO-3306 (control) in complex with CDK1. The stability and flexibility of the protein−ligand complexes in a body microenvironment in terms of solvation, ions, pressure, and temperature were assessed through a 100 ns MD run. This was achieved by looking into the potential energies, the radius of gyration (RoG), RMSD, RMSF, and hydrogen bonds between the protein residues, as well as between the ligand and the protein from the resulting trajectories.

The potential energies of the selected hits were analyzed compared to the control RO-3306 in a complex with CDK1. They were found to be energetically stable throughout the 100 ns MD run as depicted in the Energy plots in Figure 5A, Figure 6A, Figure S10A, and Figure S11A. RoG determines the compactness of the protein complexes; a high radius of gyration leads to instability and a loss of the compact structure. Compounds selected from both DrugBank and Otava libraries performed satisfactorily and exhibited stable RoG curves (Figure 5B and Figure 6B). The complexes CDK1-DB_1 and CDK1-DB_6 acquired lower RoG values than the control RO-3306 while CDK1-DB_7, apart from a slight jump around 50 ns, was almost stable throughout the trajectory. All five hits from the Otava libraries had stable RoG throughout 100 ns, where CDK1-OT_17, CDK1-OT_2, and CDK1-OT_1 illustrated lower RoG values as compared to the control, suggesting greater compactness of the complexes. IH_9 and IH_10 maintained the compactness of their respective complex as shown in Figure S10B. The RMSD evaluation of a ligand-protein complex gives insight into the stability in terms of structural deviations when the ligand binds to the protein versus the unbound protein. From the RMSD plots, Figure 5C, Figure 6C, Figure S10C, and Figure 11C, CDK1-DB_1 and CDK1-DB_6 were structurally more stable than the control CDK1-RO3306 complex; however, CDK1-DB_7 was comparatively less stable than the control. All five hits from the Otava libraries IH_9 and IH_10 were more or equally stable as compared to the control CDK1-RO-3306. The RMSF pattern gives an idea about the stability of individual amino acid residues, preserving the protein complex's dynamic flexibility. All the selected hit molecules had almost stable configurations for all the active site residues in the range of 10−146 similar to the control with overall fluctuations not more than 0.5 nm (Figure 5D, Figure 6D, Figure S10D, and Figure S11D). Almost all fluctuating residues were outside the binding site of CDK1 as listed in Table S7. In addition to these criteria, hydrogen bonds within the protein and between the protein−ligand complexes indicate the rigidity of the complex. In Figure 5E-F, Figure 6E-F, Figure S10E-F, and Figure S11E-F, CDK1-DB_6 from DrugBank and CDK1-OT_11 from Otava libraries had the highest number of hydrogen bonds compared to other compounds including the control. The results from the 100 ns MD simulations suggest two ligands DB_1 and DB_6 from DrugBank, all the Otava hit compounds, and IH_9 to be stable

https://doi.org/10.1021/acsomega.4c05414
ACS Omega 2024, 9, 39873−39892

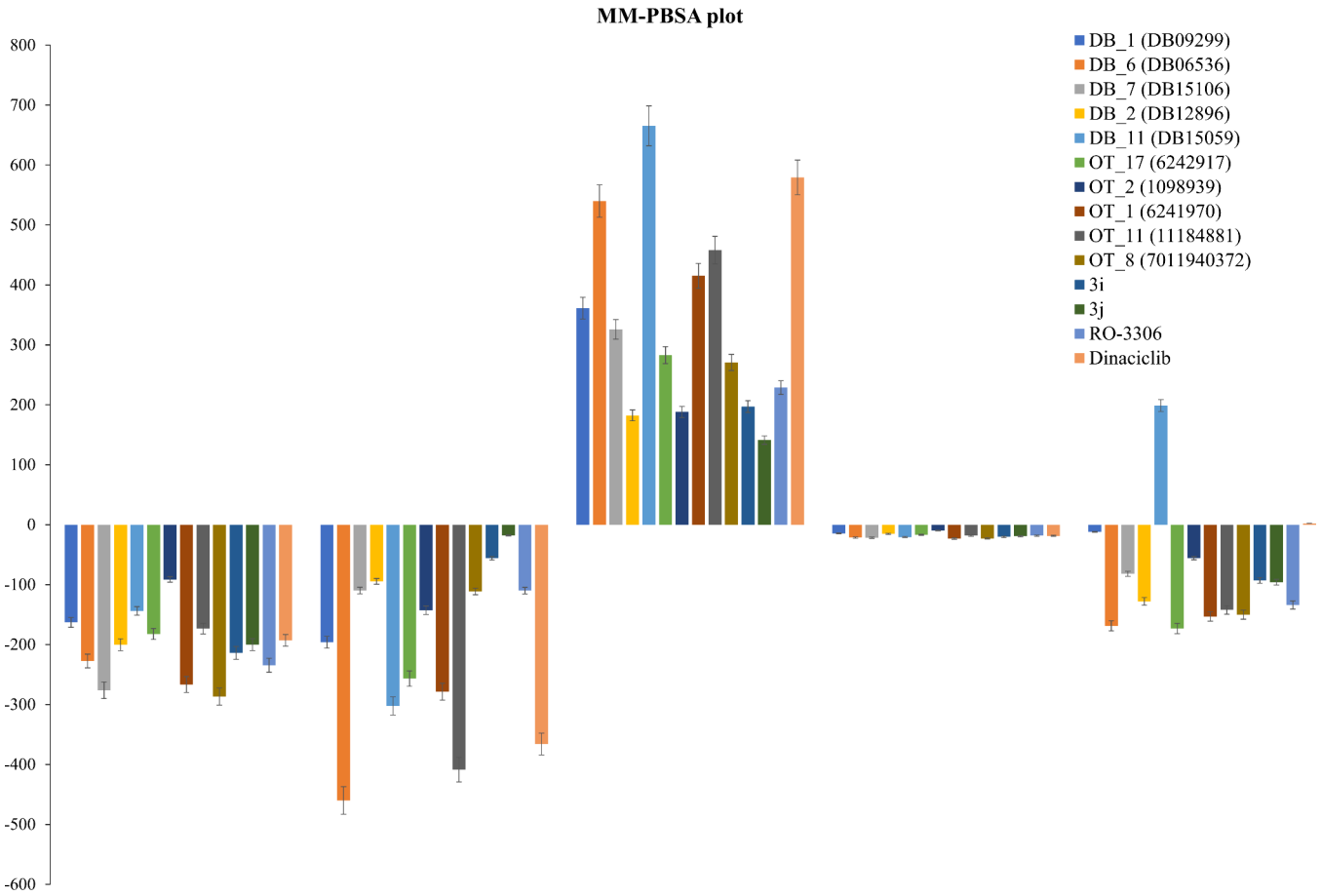

Figure 7. Binding free energy prediction for the top 10 hit compounds and the two selected in-house library compounds including controls RO-3306 and Dinaciclib with individual energy components for each compound.

Table 3. Values of the Energy Components of All 12 Hit Molecules along with Control Molecules RO-3306 and Dinaciclib by the MM-PBSA Method

C.No.	Compound Code	ΔE_{VDW} (kJ/mol)	ΔE_{ELE} (kJ/mol)	$\Delta G_{SOL\text{-}PB}$ (kJ/mol)	γ_{SASA} (kJ/mol)	$\Delta G_{bind\text{-}PBSA}$ (kJ/mol)
DB_1	DB09299	−162.89 ± 1.064	−196.043 ± 2.461	361.296 ± 4.154	−14.579 ± 0.092	−12.016 ± 2.232
DB_6	DB06536	−227.358 ± 1.337	−459.914 ± 2.273	539.869 ± 3.080	−21.457 ± 0.074	−168.69 ± 1.983
DB_7	DB15106	−276.119 ± 1.149	−109.87 ± 2.775	325.838 ± 3.421	−21.723 ± 0.087	−81.889 ± 2.106
DB_2	DB12896	−200.289 ± 0.890	−94.509 ± 1.372	182.344 ± 1.828	−15.385 ± 0.056	−127.813 ± 1.313
DB_11	DB15059	−143.861 ± 1.247	−302.216 ± 2.752	665.438 ± 3.133	−20.598 ± 0.079	198.794 ± 2.412
OT_17	6242917	−182.302 ± 0.937	−256.692 ± 3.780	282.807 ± 5.133	−16.886 ± 0.085	−173.138 ± 2.228
OT_2	1098939	−91.445 ± 0.981	−142.525 ± 6.579	188.077 ± 6.484	−9.852 ± 0.173	−55.822 ± 2.665
OT_1	6241970	−266.474 ± 1.869	−278.588 ± 3.622	415.181 ± 4.958	−23.221 ± 0.099	−153.179 ± 2.709
OT_11	11184881	−173.439 ± 1.61	−408.544 ± 2.911	458.158 ± 3.92	−18.312 ± 0.093	−142.206 ± 2.271
OT_8	7011940372	−286.668 ± 0.966	−111.212 ± 0.947	270.714 ± 1.829	−22.801 ± 0.069	−150.06 ± 1.450
IH_9	3i	−213.872 ± 0.863	−55.956 ± 1.278	197.195 ± 1.912	−20.302 ± 0.081	−93.049 ± 1.081
IH_10	3j	−199.962 ± 0.885	−17.856 ± 0.515	141.185 ± 1.091	−19.252 ± 0.081	−95.858 ± 0.936
Control	RO-3306	−234.381 ± 1.026	−110.036 ± 1.903	228.655 ± 2.988	−18.239 ± 0.078	−133.929 ± 1.383
Control	Dinaciclib	−192.900 ± 1.157	−365.863 ± 3.885	579.336 ± 4.370	−18.622 ± 0.074	2.231 ± 2.271

and effective as CDK1 inhibitors when compared to the control compound RO-3306. In addition, these parameters were also compared with other control Dinaciclib (pan CDK-inhibitor) as shown in Figure S12 and Figure S13.

3.6. Binding Free Energy Calculations and Molecular Similarity Evaluation. The binding free energy was calculated for all 12 hit molecules using the g_mmpbsa tool of GROMACS by the MM-PBSA method for the last 20 ns of the MD simulation trajectory. The binding energy is influenced by van der Waals energy, electrostatic energy, and SASA energy negatively whereas in a positive manner by polar solvation energy. As shown in Figure 7 and Table 3, the binding energy of the hits except for DB_11 (198 ± 2.412 kJ/mol) and Dinaciclib (2.231 ± 2.271 kJ/mol) was negative including the control ligand RO-3306 (−133.929 ± 1.383 kJ/mol). In the case of DB_11 and Dinaciclib, the contribution of solvation energy ($\Delta G_{SOL\text{-}PB}$ and γ_{SASA}) to the overall binding energy was found to be significantly higher compared to the van der Waals and electrostatic energies. This could be the reason for the positive binding energy value for these two

https://doi.org/10.1021/acsomega.4c05414
ACS Omega 2024, 9, 39873−39892

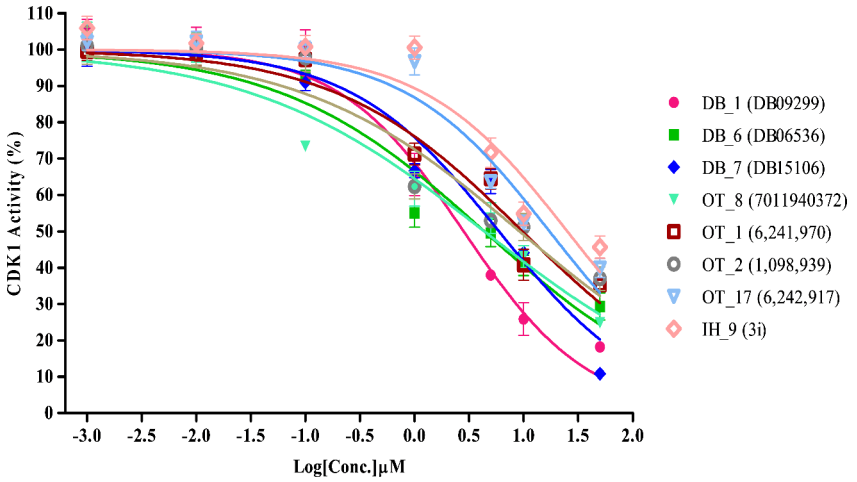

Figure 8. Seven-point percentage response curves depicting the decline in the CDK1 Activity with increasing concentrations of the final eight hit compounds for determining IC50 values using GraphPad Prism software.

molecules. The rest of the 11 hits were found to have better binding energy values compared to the controls with DrugBank hit DB_6 and Otava hit OT_17 having the best values at −168.69 ± 1.983 and −173.138 ± 2.228 kJ/mol, respectively, except DB_1 (−12.016 ± 2.232 kJ/mol), DB_7 (−81.889 ± 2.106 kJ/mol), OT_2 (−55.822 ± 2.665 kJ/mol), IH_9 (−93.049 ± 1.081 kJ/mol), and IH_10 (−95.858 ± 0.936 kJ/mol) which had comparable binding energies. This data suggests that all the 11 hits generated from the *in silico* analysis except DB_11 (with positive binding free energy) may act as potential CDK1 inhibitors.

The MMPBSA method can also be utilized to examine the energy contribution of individual residues. This process involves decomposing each residue's energy by considering the interactions in which each residue is engaged. The per-residue energy decomposition calculation for each protein−ligand complex was conducted. The binding site residues that show significant energy deviations were highlighted with green color (negative energy contribution) and red color (positive energy contribution) in the Figure S14A−D. In most of the interactions, the binding site residues Gly12, Gly13, Val18, Leu83, Met85, Leu135, and Asp146 were observed to contribute toward favorable binding energies, whereas residues Gly11, Tyr15, Ser84, Lys89, and Asn133 were considered unfavorable for ligand binding.

To further validate these hits, the molecular similarity indices for the final 12 hit molecules were compared to the control, RO-3306 using the "Molecular Similarity Search Tool" in DS 2021 by means of Tanimoto index. 10 out of the 12 hits had a Tanimoto coefficient of greater than 0.5, as indicated in Table S9 reflecting a strong structural resemblance. This suggests that the majority of the selected hits share significant structural features with known active compound, supporting their potential as viable candidates for further studies.

3.7. Kinase Assay for Potential CDK1 Inhibitors. CDK1 Kinase Assay kit from Promega was used to evaluate top 10 hit molecules selected from MD simulation studies. Known inhibitors, Dinaciclib[99,114] and RO-3306[100] were used as reference compounds for this assay. All the compounds were initially tested at two concentrations, 10 and 100 μM. In addition to these two concentrations, the reference compounds were also evaluated at 1 μM. Dinaciclib inhibited complete CDK1 activity at all three concentrations. RO-3306 showed around 20% activity at 1 μM; however, it inhibited 100% of the protein at higher concentrations. The inhibitory profile of all ten test compounds is shown in Table S8. All of the compounds except OT_11 and IH_10 showed more than 50% inhibition at 10 μM. Therefore, finally, eight compounds were then taken for determination of their inhibitory potential (IC_{50}) for CDK1.

The compounds were found to decrease the CDK1 activity with IC_{50} values in the range of 2.8−25 μM (Figure 8). Out of these eight compounds, DrugBank hits, DB_1 and DB_6, and Otava compound OT_8 were found to be most active with IC_{50} values at 2.822, 4.365, and 4.357 μM, respectively (Table 4).

Table 4. IC_{50} Values of the Final Eight Compounds Tested in the CDK1 Kinase Assay

Compound No.	Compound Details	IC_{50} (μM)
DB_1	DB09299 (tenofovir alafenamide)	2.822
DB_6	DB06536 (tesaglitazar)	4.365
OT_8	7011940372	4.357
DB_7	DB15106 (Surufatinib)	5.945
OT_2	1,098,939	9.170
OT_1	6,241,970	9.750
OT_17	6,242,917	17.27
IH_9	3i	25.16

4. DISCUSSION

CDKs have been considered an important target in the development of cancer therapeutics. Tackling the serious side effects posed by pan-inhibitors, the design and development of subtype-specific inhibitors has been the focus of research for the last two decades. In the current study, ligand-based 3D QSAR pharmacophore models were generated using the existing research data on CDK1 inhibitors and CDK4/6 inhibitors. The utilization of these pharmacophore models in the virtual screening of multiple databases for potential CDK1 inhibitors resulted in the identification of a diverse set of compounds. These compounds were then evaluated for their pharmacokinetic and pharmacodynamic properties to determine their suitability as promising drug candidates. Looking at the previous studies for the development of pharmacophore

https://doi.org/10.1021/acsomega.4c05414
ACS Omega 2024, 9, 39873−39892

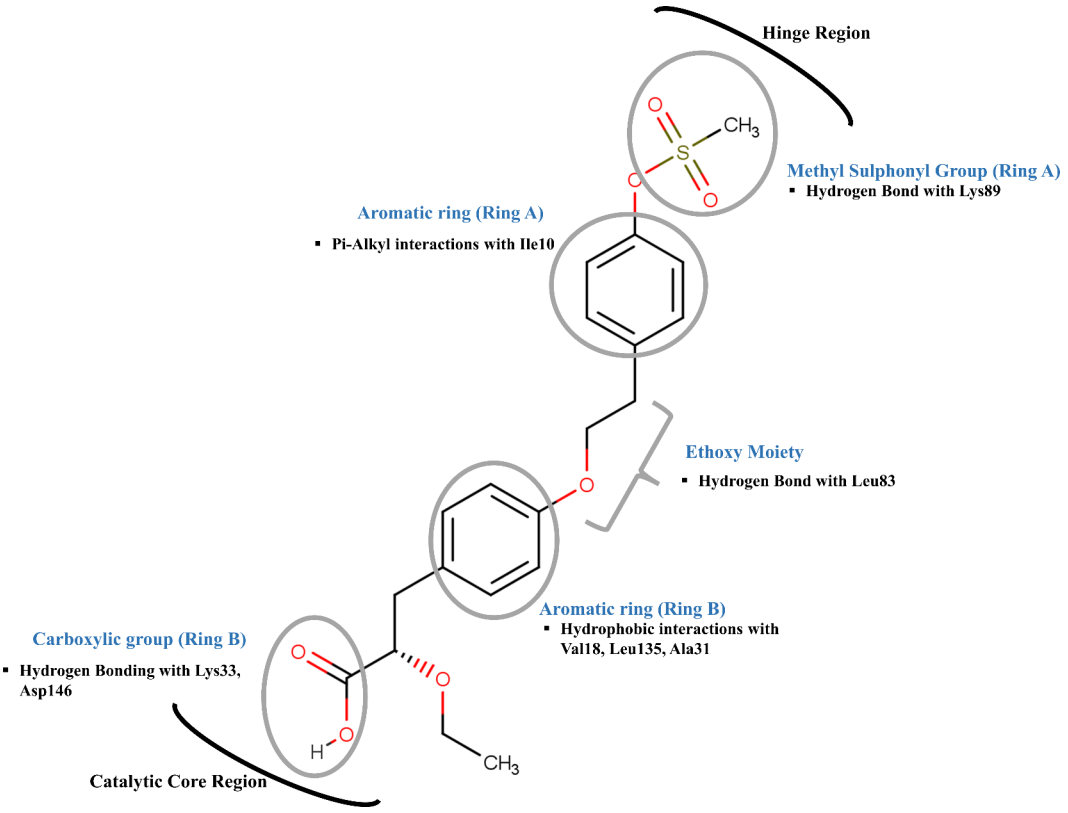

Figure 9. An illustration of the structure−activity relationship (SAR) of tesaglitazar (DB06536) depicting the important interactions among its chemical groups.

models to screen out CDK1 inhibitors,[40,41] our model Hypo_CDK1 was generated using a diverse set of compounds that exhibited different feature sets essential to be active for CDK1 and better cost values with a cost difference of 101.98. Hypo_CDK1 also showed a better correlation (0.81) between the actual and predicted activity values of the test set molecules, suggesting a high likelihood of predicting potential CDK1 inhibitors. Additionally, the screened molecules were also mapped to generated Hypo_CDK4/6 to ensure selectivity by removing the common hits based on fit values and predicted activity.

The compounds selected based on these filters were further analyzed for their binding efficiency to the CDK1 active site. A total of 10 molecules were selected as top hits that showed complex formations with CDK1 comparable to those of the control ligands, Dinaciclib and RO-3306. These compounds retained important H-bond and hydrophobic interactions with the active site residues of CDK1. Interactions with residues, namely, Phe82, Leu83, Ser84, Met85, and Asp86 were considered unique to CDK1 with a H-bond with Leu83 or Asp86 or both to be indispensable for good binding affinity to CDK1. In addition to this, an in-house synthetic library of 1,3,4-oxadiazole thiones was also mapped to Hypo_CDK1; selected compounds were docked in the binding site of CDK1 and two compounds IH_9 and IH_10 were finally selected for MD simulation studies and the *in vitro* Kinase inhibition assay.

Out of the 10 hits, three compounds, **DB_1 (DB09299)**, **DB_6 (DB06536)**, and **OT_8 (7011940372)**, resonated with the control molecules in terms of the type of interactions with the key residues. Finally, we looked into the structure−activity relationship (SAR) of these compounds (Figure 9), and we inferred that the aromatic rings in all three preserved the hydrophobic interactions (pi-pi bonds) with the solvent-exposed residues in the binding site of CDK1. DB_1 features a pyrazolopyrimidine group that mimics the pyrazolo group of ATP[11] and formed crucial hydrogen bond interactions with Leu83 and Asp86. Both DB_6 and OT_8 possess sulfonyl side chains attached to an aromatic ring outside the active site cleft at the C-terminal lobe of CDK1 that formed strong H bond interactions with the hinge region and hydrophobic interactions with Ile10. The carboxylic side chain of DB_1, the polar substituents of DB_6, and the aromatic ring of OT_8 were embedded in the active site presenting strong interactions with Val18, Lys33, Phe80, and Ala145 of the catalytic core increasing the overall potency against CDK1 as suggested in a previous research.[115] Therefore, we can estimate that the presence of an aromatic ring with sulfonamide substitution toward the C-helix in the hinge region, a second ring with polar functional groups binding to the deep catalytic domain, can provide increased selectivity to a compound as potential CDK1 inhibitors. 100 ns MD simulation studies and negative binding energies using the MM-PBSA method of these hits revealed the stable configuration of their complexes with CDK1 in the body microenvironment. *In vitro* evaluation of the final hit compounds using the CDK1 Kinase Assay provided the IC_{50} values for CDK1 inhibition. Among the DrugBank compounds, tenofovir alafenamide (DB09299), an antiviral drug used for the treatment of HIV and chronic Hepatitis B infections;[116,117] tesaglitazar (DB06536), a dual PPAR agonist indicated for the treatment of Type II diabetes,[118] were found to be most active against CDK1. The cytotoxicity profile of tenofovir alafenamide suggests that it is safe with minimal cytotoxic effects and low potential for mitochondrial toxicity.[119] Similarly, tesaglitazar was found to show no

https://doi.org/10.1021/acsomega.4c05414
ACS Omega 2024, 9, 39873−39892

significant toxicity to primary hepatocytes.[120] From the screened Otava library, compound 7011940372 was found to be most active in low micromolar range. In the case of IH_9 and IH_10, from the *in silico* results, we can infer that IH_9 is a better hit molecule compared to IH_10. It showed favorable interactions with key residues in the binding site like hydrogen bonds with Leu83 and hydrophobic interactions with the hinge region residues like Lys89 along with other pi-alkyl bonds with Ile10, Val18, Ala31 and Leu135 through the aromatic rings present. The RMSD, RMSF and hydrogen bonds of the complex also showed that IH_9 could be a better CDK1 inhibitor than IH_10. These inferences were further confirmed by the kinase inhibition assay where IH_9 was found to be more active than IH_10 with IC_{50} at 23.802 μM.

More than 80% of the final hits when compared to the control, RO-3306 showed greater than 50% similarity in the molecular structure. This concludes that the pharmacophore generated for CDK1 was robust and had good predictability to screen novel inhibitors for CDK1.

These results can be utilized to develop better-optimized inhibitors for CDK1 by understanding the required structural features for a compound to be multifold selective for a specific subtype. To date, there has been no significant success in the development of CDK1 inhibitors. Dinaciclib is a highly potent pan-CDK inhibitor but it has shown severe side effects in the clinic.[121] RO-3306 has shown promising results in the lab;[122] however, the performance of this inhibitor has not been satisfactory in the clinics and hence has been withdrawn from the trials.[38] Therefore, there is an urgent need to develop subtype-selective inhibitors for CDK1 to mitigate the hazards of pan inhibitors in cancer therapy.

5. CONCLUSION

Rapid advances in the field of anticancer therapy have led to the development of many successful drug molecules targeting the most important driving factors of oncogenic progression. One of those factors, overexpression of CDKs, has been dealt with utmost relevance in the field of research. The present work focuses on the development of potential CDK1 inhibitors using a combined *in silico* and *in vitro* approach. The top 10 hits generated with the help of computational studies and two molecules from an in-house library are validated in an *in vitro* enzyme inhibition assay to assess their effectiveness in reducing the CDK1 activity. Although, the simulation studies suggest nine of the top ten and 3i from the in-house library to be a potential candidate, we suggest that tenofovir alafenamide and tesaglitazar can be repurposed as inhibitors for CDK1 based on their lowest IC_{50} values. These findings need to be further validated by using cell-based and *in vivo* studies. Compound 7011940372 from the Otava Libraries and 3i from the in-house library can be used as a starting hit molecule to develop subtype-selective inhibitors for CDK1. This study provides a preliminary basis for the objective of the development of better and more potent inhibitors with scaffolds similar to these compounds and paves the foundation for the design and development of better drugs in the future.

■ ASSOCIATED CONTENT

Supporting Information

The Supporting Information is available free of charge at https://pubs.acs.org/doi/10.1021/acsomega.4c05414.

Chemical structures of the training and test set molecules for CDK1 and CDK4/6 pharmacophores; details of in-house library compounds; experimental and estimated IC_{50} values of training set and test set molecules based on Hypo1_CDK1 and Hypo1_CDK4/6; regression curves for training and test sets; representative ligand pharmacophore mapping for CDK4/6; Fischer validation of Hypo1_CDK4/6; ADMET analysis; superimposed redocked poses, 2D interaction maps of cocrystallized ligands (CDK1 and CDK4/6); controls IH_9 and IH_10 with CDK1; details of the final 10 hits (5 from DrugBank and 5 from Otava) selected for MD simulations along with control Dinaciclib and RO-3306); MD simulation trajectories with respect to energy, RMSF, RMSD, hydrogen bonds of IH_9 and IH_10 with CDK1, of DB_2 and DB_11 with CDK1, of Drugbank compounds with CDK1, of Otava hits with CDK1; RMS fluctuation residues of the 12 hits selected; per residue contributions to binding energy for all 12 hit molecules along with controls; percent inhibition of CDK1 for all test compounds along with controls, Dinaciclib and RO-3306 and tanimoto similarity index for the final 12 hit molecules with the control, RO-3306 (DOCX)

■ AUTHOR INFORMATION

Corresponding Author

Madhu Chopra − *Laboratory of Molecular Modeling and Anti-Cancer Drug Development, Dr. B. R. Ambedkar Center for Biomedical Research, University of Delhi, Delhi 110007, India;* orcid.org/0000-0003-3154-7335; Email: mchopradu@gmail.com

Authors

Vineeta Teotia − *Laboratory of Molecular Modeling and Anti-Cancer Drug Development, Dr. B. R. Ambedkar Center for Biomedical Research, University of Delhi, Delhi 110007, India;* orcid.org/0009-0009-7130-7361

Prakash Jha − *Laboratory of Molecular Modeling and Anti-Cancer Drug Development, Dr. B. R. Ambedkar Center for Biomedical Research, University of Delhi, Delhi 110007, India;* orcid.org/0000-0001-8951-1875

Complete contact information is available at: https://pubs.acs.org/10.1021/acsomega.4c05414

Notes

The authors declare no competing financial interest.

■ ACKNOWLEDGMENTS

This work was supported by a Grant from the Department of Biotechnology (Govt. of India) for the Establishment of Bioinformatics Centre (BIC) (BT/PR40153/BTIS/137/8/2021) National Network Project (BT/PR40195/BTIS/137/58/2023) at Dr. B. R. Ambedkar Center for Biomedical Research and the Institute Of Eminence, University of Delhi [IoE/2023-24/12/FRP]. The authors thankfully acknowledge the Bioinformatics Centre (BIC), Department of Biotechnology, Govt. of India to M.C. for *in silico* analysis; National Network Project and Institution of Eminence, University of Delhi for financial support to M.C. for *in vitro* analysis. The authors acknowledge Dr. B. R. Ambedkar Center for Biomedical Research, University of Delhi for lending

bioinformatics infrastructural facility (BIC) and Bioinformatics Resources and Applications Facility (BRAF), C-DAC, "Pune" for providing server assistance. V.T. was recipient of a Ph.D. fellowship from CSIR-NET by grant number (09/045(1642)/2019-EMR-I). P.J. is thankful for the position of Project Scientist-I under the DBT-BIC project with grant number (BT/PR40153/BTIS/137/8/2021).

REFERENCES

(1) Suski, J. M.; Braun, M.; Strmiska, V.; Sicinski, P. Targeting Cell-Cycle Machinery in Cancer. *Cancer Cell* **2021**, *39* (6), 759−778.
(2) Ajit Kumar Saxena, G. C. Targetting Cdks in Cancer: An Overview and New Insights. *J. Cancer Sci. Ther.* **2014**, *6*, 489−496.
(3) Roskoski, R. Cyclin-Dependent Protein Serine/Threonine Kinase Inhibitors as Anticancer Drugs. *Pharmacol. Res.* **2019**, *139*, 471−488.
(4) Zhang, M.; Zhang, L.; Hei, R.; Li, X.; Cai, H.; Wu, X.; Zheng, Q.; Cai, C. CDK Inhibitors in Cancer Therapy, an Overview of Recent Development. *Am. J. Cancer Res.* **2021**, *11* (5), 1913−1935.
(5) Rizzolio, F.; Tuccinardi, T.; Caligiuri, I.; Lucchetti, C.; Giordano, A. CDK Inhibitors: From the Bench to Clinical Trials. *Curr. Drug Targets* **2010**, *11* (3), 279−290.
(6) Wood, D. J.; Endicott, J. A. Structural Insights into the Functional Diversity of the CDK-Cyclin Family. *Open Biol.* **2018**, *8* (9), 180112.
(7) Malumbres, M.; Barbacid, M. Cell Cycle, CDKs and Cancer: A Changing Paradigm. *Nat. Rev. Cancer* **2009**, *9* (3), 153−166.
(8) Santamaría, D.; Barrière, C.; Cerqueira, A.; Hunt, S.; Tardy, C.; Newton, K.; Cáceres, J. F.; Dubus, P.; Malumbres, M.; Barbacid, M. Cdk1 Is Sufficient to Drive the Mammalian Cell Cycle. *Nature* **2007**, *448* (7155), 811−815.
(9) Malumbres, M.; Barbacid, M. Mammalian Cyclin-Dependent Kinases. *Trends Biochem. Sci.* **2005**, *30* (11), 630−641.
(10) Malumbres, M. Cyclin-Dependent Kinases. *Genome Biol.* **2014**, *15* (6), 122.
(11) Brown, N. R.; Korolchuk, S.; Martin, M. P.; Stanley, W. A.; Moukhametzianov, R.; Noble, M. E. M.; Endicott, J. A. CDK1 Structures Reveal Conserved and Unique Features of the Essential Cell Cycle CDK. *Nat. Commun.* **2015**, *6* (1), 6769.
(12) Enserink, J. M.; Chymkowitch, P. Cell Cycle-Dependent Transcription: The Cyclin Dependent Kinase Cdk1 Is a Direct Regulator of Basal Transcription Machineries. *Int. J. Mol. Sci.* **2022**, *23* (3), 1293.
(13) Lim, S.; Kaldis, P. Cdks, Cyclins and CKIs: Roles beyond Cell Cycle Regulation. *Development* **2013**, *140* (15), 3079−3093.
(14) Jones, M. C.; Zha, J.; Humphries, M. J. Connections between the Cell Cycle, Cell Adhesion and the Cytoskeleton. *Philos. Trans. R. Soc. B Biol. Sci.* **2019**, *374* (1779), 20180227.
(15) Odle, R. I.; Florey, O.; Ktistakis, N. T.; Cook, S. J. CDK1, the Other "Master Regulator" of Autophagy. *Trends Cell Biol.* **2021**, *31* (2), 95−107.
(16) Leal-Esteban, L. C.; Fajas, L. Cell Cycle Regulators in Cancer Cell Metabolism. *Biochim. Biophys. Acta BBA - Mol. Basis Dis.* **2020**, *1866* (5), 165715.
(17) Xie, B.; Wang, S.; Jiang, N.; Li, J. J. Cyclin B1/CDK1-Regulated Mitochondrial Bioenergetics in Cell Cycle Progression and Tumor Resistance. *Cancer Lett.* **2019**, *443*, 56−66.
(18) Kang, J.; Sergio, C. M.; Sutherland, R. L.; Musgrove, E. A. Targeting Cyclin-Dependent Kinase 1 (CDK1) but Not CDK4/6 or CDK2 Is Selectively Lethal to MYC-Dependent Human Breast Cancer Cells. *BMC Cancer* **2014**, *14* (1), 32.
(19) Deng, Y.-R.; Chen, X.-J.; Chen, W.; Wu, L.-F.; Jiang, H.-P.; Lin, D.; Wang, L.-J.; Wang, W.; Guo, S.-Q. Sp1 Contributes to Radioresistance of Cervical Cancer through Targeting G2/M Cell Cycle Checkpoint CDK1. *Cancer Manag. Res.* **2019**, *11*, 5835−5844.
(20) Tong, Y.; Huang, Y.; Zhang, Y.; Zeng, X.; Yan, M.; Xia, Z.; Lai, D. DPP3/CDK1 Contributes to the Progression of Colorectal Cancer through Regulating Cell Proliferation, Cell Apoptosis, and Cell Migration. *Cell Death Dis.* **2021**, *12* (6), 1−12.
(21) Piao, J.; Zhu, L.; Sun, J.; Li, N.; Dong, B.; Yang, Y.; Chen, L. High Expression of CDK1 and BUB1 Predicts Poor Prognosis of Pancreatic Ductal Adenocarcinoma. *Gene* **2019**, *701*, 15−22.
(22) Zou, Y.; Ruan, S.; Jin, L.; Chen, Z.; Han, H.; Zhang, Y.; Jian, Z.; Lin, Y.; Shi, N.; Jin, H. CDK1, CCNB1, and CCNB2 Are Prognostic Biomarkers and Correlated with Immune Infiltration in Hepatocellular Carcinoma. *Med. Sci. Monit.* **2020**, *26*, No. e925289.
(23) Ren, L.; Yang, Y.; Li, W.; Zheng, X.; Liu, J.; Li, S.; Yang, H.; Zhang, Y.; Ge, B.; Zhang, S.; Fu, W.; Dong, D.; Du, G.; Wang, J. CDK1 Serves as a Therapeutic Target of Adrenocortical Carcinoma via Regulating Epithelial-Mesenchymal Transition, G2/M Phase Transition, and PANoptosis. *J. Transl. Med.* **2022**, *20* (1), 444.
(24) Ying, X.; Che, X.; Wang, J.; Zou, G.; Yu, Q.; Zhang, X. CDK1 Serves as a Novel Therapeutic Target for Endometrioid Endometrial Cancer. *J. Cancer* **2021**, *12* (8), 2206−2215.
(25) Huang, Z.; Shen, G.; Gao, J. CDK1 Promotes the Stemness of Lung Cancer Cells through Interacting with Sox2. *Clin. Transl. Oncol.* **2021**, *23* (9), 1743−1751.
(26) Zhu, S.; Al-Mathkour, M.; Cao, L.; Khalafi, S.; Chen, Z.; Poveda, J.; Peng, D.; Lu, H.; Soutto, M.; Hu, T.; McDonald, O. G.; Zaika, A.; El-Rifai, W. CDK1 Bridges NF-κB and β-Catenin Signaling in Response to H. Pylori Infection in Gastric Tumorigenesis. *Cell Rep.* **2023**, *42* (1), 112005.
(27) Liu, X.; Wu, H.; Liu, Z. An Integrative Human Pan-Cancer Analysis of Cyclin-Dependent Kinase 1 (CDK1). *Cancers* **2022**, *14* (11), 2658.
(28) Smith, P. D.; O'Hare, M. J.; Park, D. S. CDKs: Taking on a Role as Mediators of Dopaminergic Loss in Parkinson's Disease. *Trends Mol. Med.* **2004**, *10* (9), 445−451.
(29) Malhotra, N.; Gupta, R.; Kumar, P. Pharmacological Relevance of CDK Inhibitors in Alzheimer's Disease. *Neurochem. Int.* **2021**, *148*, 105115.
(30) Goga, A.; Yang, D.; Tward, A. D.; Morgan, D. O.; Bishop, J. M. Inhibition of CDK1 as a Potential Therapy for Tumors Over-Expressing MYC. *Nat. Med.* **2007**, *13* (7), 820−827.
(31) Wang, Q.; Bode, A. M.; Zhang, T. Targeting CDK1 in Cancer: Mechanisms and Implications. *Npj Precis. Oncol.* **2023**, *7* (1), 1−14.
(32) Wiernik, P. H. Alvocidib (Flavopiridol) for the Treatment of Chronic Lymphocytic Leukemia. *Expert Opin. Investig. Drugs* **2016**, *25* (6), 729−734.
(33) Heptinstall, A. B.; Adiyasa, I.; Cano, C.; Hardcastle, I. R. Recent Advances in CDK Inhibitors for Cancer Therapy. *Future Med. Chem.* **2018**, *10* (11), 1369−1388.
(34) Asghar, U.; Witkiewicz, A. K.; Turner, N. C.; Knudsen, E. S. The History and Future of Targeting Cyclin-Dependent Kinases in Cancer Therapy. *Nat. Rev. Drug Discovery* **2015**, *14* (2), 130−146.
(35) Panagiotou, E.; Gomatou, G.; Trontzas, I. P.; Syrigos, N.; Kotteas, E. Cyclin-Dependent Kinase (CDK) Inhibitors in Solid Tumors: A Review of Clinical Trials. *Clin. Transl. Oncol.* **2022**, *24* (2), 161−192.
(36) Diril, M. K.; Ratnacaram, C. K.; Padmakumar, V. C.; Du, T.; Wasser, M.; Coppola, V.; Tessarollo, L.; Kaldis, P. Cyclin-Dependent Kinase 1 (Cdk1) Is Essential for Cell Division and Suppression of DNA Re-Replication but Not for Liver Regeneration. *Proc. Natl. Acad. Sci. U. S. A.* **2012**, *109* (10), 3826−3831.
(37) Lau, H. W.; Ma, H. T.; Yeung, T. K.; Tam, M. Y.; Zheng, D.; Chu, S. K.; Poon, R. Y. C. Quantitative Differences between Cyclin-Dependent Kinases Underlie the Unique Functions of CDK1 in Human Cells. *Cell Rep.* **2021**, *37* (2), 109808.
(38) Johnson, N.; Li, Y.-C.; Walton, Z. E.; Cheng, K. A.; Li, D.; Rodig, S. J.; Moreau, L. A.; Unitt, C.; Bronson, R. T.; Thomas, H. D.; Newell, D. R.; D'Andrea, A. D.; Curtin, N. J.; Wong, K.-K.; Shapiro, G. I. COMPROMISED CDK1 ACTIVITY SENSITIZES BRCA-PROFICIENT CANCERS TO PARP INHIBITION. *Nat. Med.* **2011**, *17* (7), 875−882.
(39) Pushpakom, S.; Iorio, F.; Eyers, P. A.; Escott, K. J.; Hopper, S.; Wells, A.; Doig, A.; Guilliams, T.; Latimer, J.; McNamee, C.; Norris,

https://doi.org/10.1021/acsomega.4c05414
ACS Omega 2024, 9, 39873−39892

A.; Sanseau, P.; Cavalla, D.; Pirmohamed, M. Drug Repurposing: Progress, Challenges and Recommendations. *Nat. Rev. Drug Discovery* **2019**, *18* (1), 41−58.
(40) Al-Sha'er, M. A.; Taha, M. O. Discovery of Novel CDK1 Inhibitors by Combining Pharmacophore Modeling, QSAR Analysis and in Silico Screening Followed by in Vitro Bioassay. *Eur. J. Med. Chem.* **2010**, *45* (9), 4316−4330.
(41) Dong, X.; Yan, J.; Du, L.; Wu, P.; Huang, S.; Liu, T.; Hu, Y. Pharmacophore Identification, Docking and "in Silico" Screening for Novel CDK1 Inhibitors. *J. Mol. Graph. Model.* **2012**, *37*, 77−86.
(42) Navarro-Retamal, C.; Caballero, J. Flavonoids as CDK1 Inhibitors: Insights in Their Binding Orientations and Structure-Activity Relationship. *PLoS One* **2016**, *11* (8), No. e0161111.
(43) Saikat, A. S. M. An In Silico Approach for Potential Natural Compounds as Inhibitors of Protein CDK1/Cks2. *Chem. Proc.* **2021**, *8* (1), 5.
(44) Wang, J.; Zhu, W.; Tu, J.; Zheng, Y. Identification and Validation of Novel Biomarkers and Potential Targeted Drugs in Cholangiocarcinoma: Bioinformatics, Virtual Screening, and Biological Evaluation. *J. Microbiol. Biotechnol.* **2022**, *32* (10), 1262−1274.
(45) Vaghasia, H.; Sakaria, S.; Prajapati, J.; Saraf, M.; Rawal, R. M. Interactive Bioinformatics Analysis for the Screening of Hub Genes and Molecular Docking of Phytochemicals Present in Kitchen Spices to Inhibit CDK1 in Cervical Cancer. *Comput. Biol. Med.* **2022**, *149*, 105994.
(46) Sofi, S.; Mehraj, U.; Qayoom, H.; Aisha, S.; Almilaibary, A.; Alkhanani, M.; Mir, M. A. Targeting Cyclin-Dependent Kinase 1 (CDK1) in Cancer: Molecular Docking and Dynamic Simulations of Potential CDK1 Inhibitors. *Med. Oncol.* **2022**, *39* (9), 133.
(47) He, F.; Wang, X.; Wu, Q.; Liu, S.; Cao, Y.; Guo, X.; Yin, S.; Yin, N.; Li, B.; Fang, M. Identification of Potential ATP-Competitive Cyclin-Dependent Kinase 1 Inhibitors: De Novo Drug Generation, Molecular Docking, and Molecular Dynamics Simulation. *Comput. Biol. Med.* **2023**, *155*, 106645.
(48) Wishart, D. S.; Feunang, Y. D.; Guo, A. C.; Lo, E. J.; Marcu, A.; Grant, J. R.; Sajed, T.; Johnson, D.; Li, C.; Sayeeda, Z.; Assempour, N.; Iynkkaran, I.; Liu, Y.; Maciejewski, A.; Gale, N.; Wilson, A.; Chin, L.; Cummings, R.; Le, D.; Pon, A.; Knox, C.; Wilson, M. DrugBank 5.0: A Major Update to the DrugBank Database for 2018. *Nucleic Acids Res.* **2018**, *46* (D1), D1074−D1082.
(49) Compound Libraries/Screening Libraries for HTS. https://www.selleckchem.com/screening-libraries.html (accessed 2023−08−25).
(50) OTAVA chemicals, Ltd. synthetic organic compounds for research and drug discovery. https://otavachemicals.com/home (accessed 2023−08−23).
(51) Yadav, N.; Kumar, P.; Chhikara, A.; Chopra, M. Development of 1,3,4-Oxadiazole Thione Based Novel Anticancer Agents: Design, Synthesis and in-Vitro Studies. *Biomed. Pharmacother.* **2017**, *95*, 721−730.
(52) Van Der Spoel, D.; Lindahl, E.; Hess, B.; Groenhof, G.; Mark, A. E.; Berendsen, H. J. C. GROMACS: Fast, Flexible, and Free. *J. Comput. Chem.* **2005**, *26* (16), 1701−1718.
(53) Lindahl, E.; Abraham, M. J.; Hess, B.; van der Spoel, D. *GROMACS 2019.2 Source Code*, 2019. DOI: 10.5281/zenodo.2636382.
(54) Marvin was used for drawing, displaying and characterizing chemical structures, substructures and reactions: *Marvin* 19.20.0, 2019. https://chemaxon.com/marvin.
(55) Chopra, M.; Mishra, A. K. Ligand-Based Molecular Modeling Study on a Chemically Diverse Series of Cholecystokinin-B/Gastrin Receptor Antagonists: Generation of Predictive Model. *J. Chem. Inf. Model.* **2005**, *45* (6), 1934−1942.
(56) Lin, R.; Connolly, P. J.; Huang, S.; Wetter, S. K.; Lu, Y.; Murray, W. V.; Emanuel, S. L.; Gruninger, R. H.; Fuentes-Pesquera, A. R.; Rugg, C. A.; Middleton, S. A.; Jolliffe, L. K. 1-Acyl-1H-[1,2,4]Triazole-3,5-Diamine Analogues as Novel and Potent Anticancer Cyclin-Dependent Kinase Inhibitors: Synthesis and Evaluation of Biological Activities. *J. Med. Chem.* **2005**, *48* (13), 4208−4211.
(57) Havlíček, L.; Hanuš, J.; Veselý, J.; Leclerc, S.; Meijer, L.; Shaw, G.; Strnad, M. Cytokinin-Derived Cyclin-Dependent Kinase Inhibitors: Synthesis and Cdc2 Inhibitory Activity of Olomoucine and Related Compounds. *J. Med. Chem.* **1997**, *40* (4), 408−412.
(58) Wilson, S. C.; Atrash, B.; Barlow, C.; Eccles, S.; Fischer, P. M.; Hayes, A.; Kelland, L.; Jackson, W.; Jarman, M.; Mirza, A.; Moreno, J.; Nutley, B. P.; Raynaud, F. I.; Sheldrake, P.; Walton, M.; Westwood, R.; Whittaker, S.; Workman, P.; McDonald, E. Design, Synthesis and Biological Evaluation of 6-Pyridylmethylaminopurines as CDK Inhibitors. *Bioorg. Med. Chem.* **2011**, *19* (22), 6949−6965.
(59) Zhang, L.; Fan, J.; Chong, J.-H.; Cesena, A.; Tam, B. Y. Y.; Gilson, C.; Boykin, C.; Wang, D.; Aivazian, D.; Marcotte, D.; Xiao, G.; Le Brazidec, J.-Y.; Piao, J.; Lundgren, K.; Hong, K.; Vu, K.; Nguyen, K.; Gan, L.-S.; Silvian, L.; Ling, L.; Teng, M.; Reff, M.; Takeda, N.; Timple, N.; Wang, Q.; Morena, R.; Khan, S.; Zhao, S.; Li, T.; Lee, W.-C.; Taveras, A. G.; Chao, J. Design, Synthesis, and Biological Evaluation of Pyrazolopyrimidine-Sulfonamides as Potent Multiple-Mitotic Kinase (MMK) Inhibitors (Part I). *Bioorg. Med. Chem. Lett.* **2011**, *21* (18), 5633−5637.
(60) Tadesse, S.; Bantie, L.; Tomusange, K.; Yu, M.; Islam, S.; Bykovska, N.; Noll, B.; Zhu, G.; Li, P.; Lam, F.; Kumarasiri, M.; Milne, R.; Wang, S. Discovery and Pharmacological Characterization of a Novel Series of Highly Selective Inhibitors of Cyclin-Dependent Kinases 4 and 6 as Anticancer Agents. *Br. J. Pharmacol.* **2018**, *175* (12), 2399−2413.
(61) Fu, Y.; Tang, S.; Su, Y.; Lan, X.; Ye, Y.; Zha, C.; Li, L.; Cao, J.; Chen, Y.; Jiang, L.; Huang, Y.; Ding, J.; Geng, M.; Huang, M.; Wan, H. Discovery of a Class of Diheteroaromatic Amines as Orally Bioavailable CDK1/4/6 Inhibitors. *Bioorg. Med. Chem. Lett.* **2017**, *27* (23), 5332−5336.
(62) Wang, S.; Midgley, C. A.; Scaërou, F.; Grabarek, J. B.; Griffiths, G.; Jackson, W.; Kontopidis, G.; McClue, S. J.; McInnes, C.; Meades, C.; Mezna, M.; Plater, A.; Stuart, I.; Thomas, M. P.; Wood, G.; Clarke, R. G.; Blake, D. G.; Zheleva, D. I.; Lane, D. P.; Jackson, R. C.; Glover, D. M.; Fischer, P. M. Discovery of N-Phenyl-4-(Thiazol-5-Yl)Pyrimidin-2-Amine Aurora Kinase Inhibitors. *J. Med. Chem.* **2010**, *53* (11), 4367−4378.
(63) Logé, C.; Testard, A.; Thiéry, V.; Lozach, O.; Blairvacq, M.; Robert, J.-M.; Meijer, L.; Besson, T. Novel 9-Oxo-Thiazolo[5,4-f]Quinazoline-2-Carbonitrile Derivatives as Dual Cyclin-Dependent Kinase 1 (CDK1)/Glycogen Synthase Kinase-3 (GSK-3) Inhibitors: Synthesis, Biological Evaluation and Molecular Modeling Studies. *Eur. J. Med. Chem.* **2008**, *43* (7), 1469−1477.
(64) Schultz, C.; Link, A.; Leost, M.; Zaharevitz, D. W.; Gussio, R.; Sausville, E. A.; Meijer, L.; Kunick, C. Paullones, a Series of Cyclin-Dependent Kinase Inhibitors: Synthesis, Evaluation of CDK1/Cyclin B Inhibition, and in Vitro Antitumor Activity. *J. Med. Chem.* **1999**, *42* (15), 2909−2919.
(65) Apel, C.; Dumontet, V.; Lozach, O.; Meijer, L.; Guéritte, F.; Litaudon, M. Phenanthrene Derivatives from Appendicula Reflexa as New CDK1/Cyclin B Inhibitors. *Phytochem. Lett.* **2012**, *5* (4), 814−818.
(66) Schoepfer, J.; Fretz, H.; Chaudhuri, B.; Muller, L.; Seeber, E.; Meijer, L.; Lozach, O.; Vangrevelinghe, E.; Furet, P. Structure-Based Design and Synthesis of 2-Benzylidene-Benzofuran-3-Ones as Flavopiridol Mimics. *J. Med. Chem.* **2002**, *45* (9), 1741−1747.
(67) Sayle, K. L.; Bentley, J.; Boyle, F. T.; Calvert, A. H.; Cheng, Y.; Curtin, N. J.; Endicott, J. A.; Golding, B. T.; Hardcastle, I. R.; Jewsbury, P.; Mesguiche, V.; Newell, D. R.; Noble, M. E. M.; Parsons, R. J.; Pratt, D. J.; Wang, L. Z.; Griffin, R. J. Structure-Based Design of 2-Arylamino-4-Cyclohexylmethyl-5-Nitroso-6-Aminopyrimidine Inhibitors of Cyclin-Dependent Kinases 1 and 2. *Bioorg. Med. Chem. Lett.* **2003**, *13* (18), 3079−3082.
(68) Chen, S.; Chen, L.; Le, N. T.; Zhao, C.; Sidduri, A.; Lou, J. P.; Michoud, C.; Portland, L.; Jackson, N.; Liu, J.-J.; et al. Synthesis and Activity of Quinolinyl-Methylene-Thiazolinones as Potent and Selective Cyclin-Dependent Kinase 1 Inhibitors. *Bioorg. Med. Chem. Lett.* **2007**, *17* (8), 2134−2138.

https://doi.org/10.1021/acsomega.4c05414
ACS Omega 2024, 9, 39873−39892

(69) Misra, R. N.; Xiao, H.; Williams, D. K.; Kim, K. S.; Lu, S.; Keller, K. A.; Mulheron, J. G.; Batorsky, R.; Tokarski, J. S.; Sack, J. S.; Kimball, S. D.; Lee, F. Y.; Webster, K. R. Synthesis and Biological Activity of N-Aryl-2-Aminothiazoles: Potent Pan Inhibitors of Cyclin-Dependent Kinases. *Bioorg. Med. Chem. Lett.* **2004**, *14* (11), 2973−2977.
(70) Lee, J.; Choi, H.; Kim, K.-H.; Jeong, S.; Park, J.-W.; Baek, C.-S.; Lee, S.-H. Synthesis and Biological Evaluation of 3,5-Diaminoindazoles as Cyclin-Dependent Kinase Inhibitors. *Bioorg. Med. Chem. Lett.* **2008**, *18* (7), 2292−2295.
(71) Le Brazidec, J.-Y.; Pasis, A.; Tam, B.; Boykin, C.; Black, C.; Wang, D.; Claassen, G.; Chong, J.-H.; Chao, J.; Fan, J.; Nguyen, K.; Silvian, L.; Ling, L.; Zhang, L.; Choi, M.; Teng, M.; Pathan, N.; Zhao, S.; Li, T.; Taveras, A. Synthesis, SAR and Biological Evaluation of 1,6-Disubstituted-1H-Pyrazolo[3,4-d]Pyrimidines as Dual Inhibitors of Aurora Kinases and CDK1. *Bioorg. Med. Chem. Lett.* **2012**, *22* (5), 2070−2074.
(72) Cho, Y. S.; Borland, M.; Brain, C.; Chen, C. H.-T.; Cheng, H.; Chopra, R.; Chung, K.; Groarke, J.; He, G.; Hou, Y.; Kim, S.; Kovats, S.; Lu, Y.; O'Reilly, M.; Shen, J.; Smith, T.; Trakshel, G.; Vögtle, M.; Xu, M.; Xu, M.; Sung, M. J. 4-(Pyrazol-4-Yl)-Pyrimidines as Selective Inhibitors of Cyclin-Dependent Kinase 4/6. *J. Med. Chem.* **2010**, *53* (22), 7938−7957.
(73) Wang, Y.; Liu, W.-J.; Yin, L.; Li, H.; Chen, Z.-H.; Zhu, D.-X.; Song, X.-Q.; Cheng, Z.-Z.; Song, P.; Wang, Z.; Li, Z.-G. Design and Synthesis of 4-(2,3-Dihydro-1H-Benzo[d]Pyrrolo[1,2-a]Imidazol-7-Yl)-N-(5-(Piperazin-1-Ylmethyl)Pyridine-2-Yl)Pyrimidin-2-Amine as a Highly Potent and Selective Cyclin-Dependent Kinases 4 and 6 Inhibitors and the Discovery of Structure-Activity Relationships. *Bioorg. Med. Chem. Lett.* **2018**, *28* (5), 974−978.
(74) Jenkins, P. R.; Wilson, J.; Emmerson, D.; Garcia, M. D.; Smith, M. R.; Gray, S. J.; Britton, R. G.; Mahale, S.; Chaudhuri, B. Design, Synthesis and Biological Evaluation of New Tryptamine and Tetrahydro-β-Carboline-Based Selective Inhibitors of CDK4. *Bioorg. Med. Chem.* **2008**, *16* (16), 7728−7739.
(75) Zha, C.; Deng, W.; Fu, Y.; Tang, S.; Lan, X.; Ye, Y.; Su, Y.; Jiang, L.; Chen, Y.; Huang, Y.; Ding, J.; Geng, M.; Huang, M.; Wan, H. Design, Synthesis and Biological Evaluation of Tetrahydronaphthyridine Derivatives as Bioavailable CDK4/6 Inhibitors for Cancer Therapy. *Eur. J. Med. Chem.* **2018**, *148*, 140−153.
(76) Jiang, B.; Wang, E. S.; Donovan, K. A.; Liang, Y.; Fischer, E. S.; Zhang, T.; Gray, N. S. Development of Dual and Selective Degraders of Cyclin-Dependent Kinases 4 and 6. *Angew. Chem., Int. Ed.* **2019**, *58* (19), 6321−6326.
(77) Tadesse, S.; Bantie, L.; Tomusange, K.; Yu, M.; Islam, S.; Bykovska, N.; Noll, B.; Zhu, G.; Li, P.; Lam, F.; Kumarasiri, M.; Milne, R.; Wang, S. Discovery and Pharmacological Characterization of a Novel Series of Highly Selective Inhibitors of Cyclin-Dependent Kinases 4 and 6 as Anticancer Agents. *Br. J. Pharmacol.* **2018**, *175* (12), 2399−2413.
(78) Shi, C.; Wang, Q.; Liao, X.; Ge, H.; Huo, G.; Zhang, L.; Chen, N.; Zhai, X.; Hong, Y.; Wang, L.; Han, Y.; Xiao, W.; Wang, Z.; Shi, W.; Mao, Y.; Yu, J.; Xia, G.; Liu, Y. Discovery of 6-(2-(Dimethylamino)Ethyl)-N-(5-Fluoro-4-(4-Fluoro-1-Isopropyl-2-Methyl-1H-Benzo[d]Imidazole-6-Yl)Pyrimidin-2-Yl)-5,6,7,8-Tetrahydro-1,6-Naphthyridin-2-Amine as a Highly Potent Cyclin-Dependent Kinase 4/6 Inhibitor for Treatment of Cancer. *Eur. J. Med. Chem.* **2019**, *178*, 352−364.
(79) Horiuchi, T.; Nagata, M.; Kitagawa, M.; Akahane, K.; Uoto, K. Discovery of Novel Thieno[2,3-d]Pyrimidin-4-Yl Hydrazone-Based Inhibitors of Cyclin D1-CDK4: Synthesis, Biological Evaluation and Structure-Activity Relationships. Part 2. *Bioorg. Med. Chem.* **2009**, *17* (23), 7850−7860.
(80) Aubry, C.; Wilson, A. J.; Emmerson, D.; Murphy, E.; Chan, Y. Y.; Dickens, M. P.; García, M. D.; Jenkins, P. R.; Mahale, S.; Chaudhuri, B. Fascaplysin-Inspired Diindolyls as Selective Inhibitors of CDK4/Cyclin D1. *Bioorg. Med. Chem.* **2009**, *17* (16), 6073−6084.
(81) VanderWel, S. N.; Harvey, P. J.; McNamara, D. J.; Repine, J. T.; Keller, P. R.; Quin, J.; Booth, R. J.; Elliott, W. L.; Dobrusin, E. M.; Fry, D. W.; Toogood, P. L. Pyrido[2,3-d]Pyrimidin-7-Ones as Specific Inhibitors of Cyclin-Dependent Kinase 4. *J. Med. Chem.* **2005**, *48* (7), 2371−2387.
(82) Markwalder, J. A.; Arnone, M. R.; Benfield, P. A.; Boisclair, M.; Burton, C. R.; Chang, C.-H.; Cox, S. S.; Czerniak, P. M.; Dean, C. L.; Doleniak, D.; Grafstrom, R.; Harrison, B. A.; Kaltenbach, R. F.; Nugiel, D. A.; Rossi, K. A.; Sherk, S. R.; Sisk, L. M.; Stouten, P.; Trainor, G. L.; Worland, P.; Seitz, S. P. Synthesis and Biological Evaluation of 1-Aryl-4,5-Dihydro-1H-Pyrazolo[3,4-d]Pyrimidin-4-One Inhibitors of Cyclin-Dependent Kinases. *J. Med. Chem.* **2004**, *47* (24), 5894−5911.
(83) Nugiel, D. A.; Etzkorn, A.-M.; Vidwans, A.; Benfield, P. A.; Boisclair, M.; Burton, C. R.; Cox, S.; Czerniak, P. M.; Doleniak, D.; Seitz, S. P. Indenopyrazoles as Novel Cyclin Dependent Kinase (CDK) Inhibitors. *J. Med. Chem.* **2001**, *44* (9), 1334−1336.
(84) Poonia, P.; Sharma, M.; Jha, P.; Chopra, M. Pharmacophore-Based Virtual Screening of ZINC Database, Molecular Modeling and Designing New Derivatives as Potential HDAC6 Inhibitors. *Mol. Divers.* **2023**, *27*, 2053.
(85) Chopra, M.; Gupta, R.; Gupta, S.; Saluja, D. Molecular Modeling Study on Chemically Diverse Series of Cyclooxygenase-2 Selective Inhibitors: Generation of Predictive Pharmacophore Model Using Catalyst. *J. Mol. Model.* **2008**, *14* (11), 1087−1099.
(86) AlQudah, D. A.; Zihlif, M. A.; Taha, M. O. Ligand-Based Modeling of Diverse Aryalkylamines Yields New Potent P-Glycoprotein Inhibitors. *Eur. J. Med. Chem.* **2016**, *110*, 204−223.
(87) John, S.; Thangapandian, S.; Arooj, M.; Hong, J. C.; Kim, K. D.; Lee, K. W. Development, Evaluation and Application of 3D QSAR Pharmacophore Model in the Discovery of Potential Human Renin Inhibitors. *BMC Bioinformatics* **2011**, *12* (14), S4.
(88) Pal, S.; Kumar, V.; Kundu, B.; Bhattacharya, D.; Preethy, N.; Reddy, M. P.; Talukdar, A. Ligand-Based Pharmacophore Modeling, Virtual Screening and Molecular Docking Studies for Discovery of Potential Topoisomerase I Inhibitors. *Comput. Struct. Biotechnol. J.* **2019**, *17*, 291−310.
(89) Kandakatla, N.; Ramakrishnan, G. Ligand Based Pharmacophore Modeling and Virtual Screening Studies to Design Novel HDAC2 Inhibitors. *Adv. Bioinform.* **2014**, *2014*, No. e812148.
(90) Kralj, S.; Jukič, M.; Bren, U. Molecular Filters in Medicinal Chemistry. *Encyclopedia* **2023**, *3* (2), 501−511.
(91) Alam, S.; Khan, F. Virtual Screening, Docking, ADMET and System Pharmacology Studies on Garcinia Caged Xanthone Derivatives for Anticancer Activity. *Sci. Rep.* **2018**, *8* (1), 5524.
(92) Coxon, C. R.; Anscombe, E.; Harnor, S. J.; Martin, M. P.; Carbain, B.; Golding, B. T.; Hardcastle, I. R.; Harlow, L. K.; Korolchuk, S.; Matheson, C. J.; Newell, D. R.; Noble, M. E. M.; Sivaprakasam, M.; Tudhope, S. J.; Turner, D. M.; Wang, L. Z.; Wedge, S. R.; Wong, C.; Griffin, R. J.; Endicott, J. A.; Cano, C. Cyclin-Dependent Kinase (CDK) Inhibitors: Structure-Activity Relationships and Insights into the CDK-2 Selectivity of 6-Substituted 2-Arylaminopurines. *J. Med. Chem.* **2017**, *60* (5), 1746−1767.
(93) Chen, P.; Lee, N. V.; Hu, W.; Xu, M.; Ferre, R. A.; Lam, H.; Bergqvist, S.; Solowiej, J.; Diehl, W.; He, Y.-A.; Yu, X.; Nagata, A.; VanArsdale, T.; Murray, B. W. Spectrum and Degree of CDK Drug Interactions Predicts Clinical Performance. *Mol. Cancer Ther.* **2016**, *15* (10), 2273−2281.
(94) RCSB PDB: Homepage. https://www.rcsb.org/ (accessed 2023−11−21).
(95) Berman, H.; Henrick, K.; Nakamura, H. Announcing the Worldwide Protein Data Bank. *Nat. Struct. Mol. Biol.* **2003**, *10* (12), 980−980.
(96) Dong, J.; Wang, X. Identification of Novel BRD4 Inhibitors by Pharmacophore Screening, Molecular Docking, and Molecular Dynamics Simulation. *J. Mol. Struct.* **2023**, *1274*, 134363.
(97) Zubair, M. S.; Maulana, S.; Widodo, A.; Mukaddas, A.; Pitopang, R. Docking Study on Anti-HIV-1 Activity of Secondary Metabolites from Zingiberaceae Plants. *J. Pharm. Bioallied Sci.* **2020**, *12*, 763.

https://doi.org/10.1021/acsomega.4c05414
ACS Omega 2024, 9, 39873−39892

(98) Paliwal, S.; Mittal, A.; Sharma, M.; pandey, A.; Singh, A.; Paliwal, S. Pharmacophore and Molecular Docking Based Identification of Novel Structurally Diverse PDE-5 Inhibitors. *Med. Chem. Res.* **2015**, *24* (2), 576−587.
(99) Paruch, K.; Dwyer, M. P.; Alvarez, C.; Brown, C.; Chan, T.-Y.; Doll, R. J.; Keertikar, K.; Knutson, C.; McKittrick, B.; Rivera, J.; Rossman, R.; Tucker, G.; Fischmann, T.; Hruza, A.; Madison, V.; Nomeir, A. A.; Wang, Y.; Kirschmeier, P.; Lees, E.; Parry, D.; Sgambellone, N.; Seghezzi, W.; Schultz, L.; Shanahan, F.; Wiswell, D.; Xu, X.; Zhou, Q.; James, R. A.; Paradkar, V. M.; Park, H.; Rokosz, L. R.; Stauffer, T. M.; Guzi, T. J. Discovery of Dinaciclib (SCH 727965): A Potent and Selective Inhibitor of Cyclin-Dependent Kinases. *ACS Med. Chem. Lett.* **2010**, *1* (5), 204−208.
(100) Vassilev, L. T.; Tovar, C.; Chen, S.; Knezevic, D.; Zhao, X.; Sun, H.; Heimbrook, D. C.; Chen, L. Selective Small-Molecule Inhibitor Reveals Critical Mitotic Functions of Human CDK1. *Proc. Natl. Acad. Sci. U. S. A.* **2006**, *103* (28), 10660−10665.
(101) Rampogu, S.; Baek, A.; Son, M.; Park, C.; Yoon, S.; Parate, S.; Lee, K. W. Discovery of Lonafarnib-Like Compounds: Pharmacophore Modeling and Molecular Dynamics Studies. *ACS Omega* **2020**, *5* (4), 1773−1781.
(102) Jha, P.; Saluja, D.; Chopra, M. Structure-Guided Pharmacophore Based Virtual Screening, Docking, and Molecular Dynamics to Discover Repurposed Drugs as Novel Inhibitors against Endoribonuclease Nsp15 of SARS-CoV-2. *J. Biomol. Struct. Dyn.* **2022**, *41* (11), 5096−5106.
(103) Schüttelkopf, A. W.; van Aalten, D. M. F. PRODRG: A Tool for High-Throughput Crystallography of Protein-Ligand Complexes. *Acta Crystallogr. D Biol. Crystallogr.* **2004**, *60* (8), 1355−1363.
(104) Hess, B.; Bekker, H.; Berendsen, H. J. C.; Fraaije, J. G. E. M. LINCS: A Linear Constraint Solver for Molecular Simulations. *J. Comput. Chem.* **1997**, *18* (12), 1463−1472.
(105) Kumari, R.; Kumar, R.; Lynn, A. G_mmpbsa—A GROMACS Tool for High-Throughput MM-PBSA Calculations. *J. Chem. Inf. Model.* **2014**, *54* (7), 1951−1962.
(106) Kollman, P. A.; Massova, I.; Reyes, C.; Kuhn, B.; Huo, S.; Chong, L.; Lee, M.; Lee, T.; Duan, Y.; Wang, W.; Donini, O.; Cieplak, P.; Srinivasan, J.; Case, D. A.; Cheatham, T. E. Calculating Structures and Free Energies of Complex Molecules: Combining Molecular Mechanics and Continuum Models. *Acc. Chem. Res.* **2000**, *33* (12), 889−897.
(107) Bajusz, D.; Rácz, A.; Héberger, K. Why is Tanimoto index an appropriate choice for fingerprint-based similarity calculations? *J. Cheminform.* **2015**, *7*, No. 20.
(108) Ohana, R. F.; Hurst, R.; Vidugiriene, J.; Slater, M. R.; Wood, K. V.; Urh, M. HaloTag-Based Purification of Functional Human Kinases from Mammalian Cells. *Protein Expr. Purif.* **2011**, *76* (2), 154−164.
(109) Tai, A. W.; Bojjireddy, N.; Balla, T. A Homogeneous and Nonisotopic Assay for Phosphatidylinositol 4-Kinases. *Anal. Biochem.* **2011**, *417* (1), 97−102.
(110) Patel, P. R.; Sun, H.; Li, S. Q.; Shen, M.; Khan, J.; Thomas, C. J.; Davis, M. I. Identification of Potent Yes1 Kinase Inhibitors Using a Library Screening Approach. *Bioorg. Med. Chem. Lett.* **2013**, *23* (15), 4398−4403.
(111) Zhu, J.; Wu, Y.; Wang, M.; Li, K.; Xu, L.; Chen, Y.; Cai, Y.; Jin, J. Integrating Machine Learning-Based Virtual Screening With Multiple Protein Structures and Bio-Assay Evaluation for Discovery of Novel GSK3β Inhibitors. *Front. Pharmacol.* **2020**, *11*, 566058.
(112) Cho, Y. S.; Borland, M.; Brain, C.; Chen, C. H.-T.; Cheng, H.; Chopra, R.; Chung, K.; Groarke, J.; He, G.; Hou, Y.; Kim, S.; Kovats, S.; Lu, Y.; O'Reilly, M.; Shen, J.; Smith, T.; Trakshel, G.; Vögtle, M.; Xu, M.; Xu, M.; Sung, M. J. 4-(Pyrazol-4-Yl)-Pyrimidines as Selective Inhibitors of Cyclin-Dependent Kinase 4/6. *J. Med. Chem.* **2010**, *53* (22), 7938−7957.
(113) Chen, P.; Lee, N. V.; Hu, W.; Xu, M.; Ferre, R. A.; Lam, H.; Bergqvist, S.; Solowiej, J.; Diehl, W.; He, Y.-A.; Yu, X.; Nagata, A.; VanArsdale, T.; Murray, B. W. Spectrum and Degree of CDK Drug Interactions Predicts Clinical Performance. *Mol. Cancer Ther.* **2016**, *15* (10), 2273−2281.
(114) Guha, M. Cyclin-Dependent Kinase Inhibitors Move into Phase III. *Nat. Rev. Drug Discovery* **2012**, *11* (12), 892−894.
(115) Navarro-Retamal, C.; Caballero, J. Flavonoids as CDK1 Inhibitors: Insights in Their Binding Orientations and Structure-Activity Relationship. *PLoS One* **2016**, *11* (8), No. e0161111.
(116) Ray, A. S.; Fordyce, M. W.; Hitchcock, M. J. M. Tenofovir Alafenamide: A Novel Prodrug of Tenofovir for the Treatment of Human Immunodeficiency Virus. *Antiviral Res.* **2016**, *125*, 63−70.
(117) Childs-Kean, L. M.; Egelund, E. F.; Jourjy, J. Tenofovir Alafenamide for the Treatment of Chronic Hepatitis B Mono-infection. *Pharmacotherapy* **2018**, *38* (10), 1051−1057.
(118) Quarta, C.; Stemmer, K.; Novikoff, A.; Yang, B.; Klingelhuber, F.; Harger, A.; Bakhti, M.; Bastidas-Ponce, A.; Baugé, E.; Campbell, J. E.; Capozzi, M.; Clemmensen, C.; Collden, G.; Cota, P.; Douros, J.; Drucker, D. J.; DuBois, B.; Feuchtinger, A.; Garcia-Caceres, C.; Grandl, G.; Hennuyer, N.; Herzig, S.; Hofmann, S. M.; Knerr, P. J.; Kulaj, K.; Lalloyer, F.; Lickert, H.; Liskiewicz, A.; Liskiewicz, D.; Maity, G.; Perez-Tilve, D.; Prakash, S.; Sanchez-Garrido, M. A.; Zhang, Q.; Staels, B.; Krahmer, N.; DiMarchi, R. D.; Tschöp, M. H.; Finan, B.; Müller, T. D. GLP-1-Mediated Delivery of Tesaglitazar Improves Obesity and Glucose Metabolism in Male Mice. *Nat. Metab.* **2022**, *4* (8), 1071−1083.
(119) 2.4 Nonclinical Overview: Emtricitabine/Tenofovir Alafenamide Fixed-Dose Combination (FTC/TAF [F/TAF] FDC). https://www.pmda.go.jp/drugs/2016/P20161209001/530614000_22800AMX00716_F100.pdf (accessed 2024−07−30).
(120) Rogue, A.; Lambert, C.; Jossé, R.; Antherieu, S.; Spire, C.; Claude, N.; Guillouzo, A. Comparative Gene Expression Profiles Induced by PPARγ and PPARα/γ Agonists in Human Hepatocytes. *PLoS One* **2011**, *6* (4), No. e18816.
(121) Mita, M. M.; Mita, A. C.; Moseley, J. L.; Poon, J.; Small, K. A.; Jou, Y.-M.; Kirschmeier, P.; Zhang, D.; Zhu, Y.; Statkevich, P.; Sankhala, K. K.; Sarantopoulos, J.; Cleary, J. M.; Chirieac, L. R.; Rodig, S. J.; Bannerji, R.; Shapiro, G. I. Phase 1 Safety, Pharmacokinetic and Pharmacodynamic Study of the Cyclin-Dependent Kinase Inhibitor Dinaciclib Administered Every Three Weeks in Patients with Advanced Malignancies. *Br. J. Cancer* **2017**, *117* (9), 1258−1268.
(122) Xia, Q.; Cai, Y.; Peng, R.; Wu, G.; Shi, Y.; Jiang, W. The CDK1 Inhibitor RO3306 Improves the Response of BRCA-Proficient Breast Cancer Cells to PARP Inhibition. *Int. J. Oncol.* **2014**, *44* (3), 735−744.

https://doi.org/10.1021/acsomega.4c05414
ACS Omega 2024, 9, 39873−39892